Space Sci Rev (2008) 139: 311–353
DOI 10.1007/s11214-008-9389-1

Plasma Flow and Related Phenomena in Planetary Aeronomy

Y.-J. Ma · K. Altwegg · T. Breus · M.R. Combi · T.E. Cravens · E. Kallio · S.A. Ledvina · J.G. Luhmann · S. Miller · A.F. Nagy · A.J. Ridley · D.F. Strobel

Received: 8 April 2008 / Accepted: 29 May 2008 / Published online: 2 July 2008
© Springer Science+Business Media B.V. 2008

Abstract Understanding the processes involved in the interaction of solar system bodies with plasma flows is fundamental to the entire field of space physics. The features of the interaction can be very different, depending upon the properties of the incident plasma as well as the nature of the obstacle. The properties of the atmosphere/ionosphere associated with the obstacle are of particular importance into understanding the plasma interaction process, especially for non-magnetized obstacle. This paper discusses in detail the roles of the atmosphere and ionosphere systems of plasma interaction around Venus, Mars, comets

Y.-J. Ma (✉)
IGPP, UCLA, 6877 Slichter Hall, Los Angeles, CA 90095, USA
e-mail: yingjuan@igpp.ula.edu

K. Altwegg
Physikalisches Institut, University of Bern, Sidlerstr. 5, 3012 Bern, Switzerland

T. Breus
Space Research Institute RAS, Profsoyznaya Str. 84/32, 117997 Moscow, Russia

M.R. Combi · A.F. Nagy · A.J. Ridley
University of Michigan, Space Res. Bldg., 2455 Hayward St., Ann Arbor, MI 48109, USA

T.E. Cravens
Department of Physics and Astronomy, University of Kansas, Lawrence, KS 66045, USA

E. Kallio
Finnish Meteorological Inst, Space Research Unit, Erik Palmenin aukio 1, Helsinki, SF-00101, Finland

S.A. Ledvina · J.G. Luhmann
Space Sciences Laboratory, University of California, Berkeley, CA 94720, USA

S. Miller
Department of Science and Technology Studies/Physics and Astronomy, University College London, Gower Street, London WC1E 6BT, UK

D.F. Strobel
Johns Hopkins University, 3400 N. Charles St., Baltimore, MD 21218, USA

and some particular satellites. The coupling between magnetosphere and ionosphere is also discussed for Earth and Giant planets.

Keywords Plasma flow · Interaction · Ionosphere

1 Introduction

The nature of the interaction between a fast-moving plasma and a relatively slow obstacle in the solar system has been studied for a long time, yet many of the relevant processes are still far from being fully understood. Such a fast-moving plasma can be the solar wind or the corotational plasma flow inside a planetary magnetosphere. The various obstacles include all of the planets, satellites, comets and asteroids in our solar system. The features of the interaction can be very different, depending upon the properties of the incident plasma and the nature of the obstacle. The characteristics of the atmosphere/ionosphere associated with the obstacle are of particular importance into understanding the plasma interaction process, especially for non-magnetized obstacle. The properties of the ionosphere are discussed in an accompanying paper by Witasse et al. (2008), as is the energy deposition to the ionosphere by Fox et al. (2008). Also the numerical simulations of the interaction are discussed by Ledvina et al. (2008) in this issue/book. This chapter will only focus on the ionospheric responses to the plasma flow.

1.1 Categories of Different Kind of Interactions with Fast Plasma Flows

The solar wind is a stream of fully ionized plasma, composed of high energy particles (mainly protons and electrons), which originates from the solar corona. The density, composition, temperature and flow velocity of the solar wind plasma is highly variable as is the interplanetary magnetic field frozen-in with the plasma. The solar wind plasma becomes both supersonic and super-Alfvenic tens of solar radii from the Sun. There are basically two types of planetary obstacles to the solar wind flow: the planetary magnetosphere and the planetary atmosphere/ionosphere system (here we do not include any discussion of interactions with solar system objects that have neither an atmosphere or a strong intrinsic magnetic field). In either case, the supersonic nature of the solar wind necessitates the formation of a bow shock to deflect the flow. The bow shock is a standing wave in front of an obstacle at which the supersonic plasma flow is slowed, heated, and deflected around the obstacles. The strength of this shock depends on the flow velocity of the solar wind relative to the velocity of compressible waves (denoted by the fast magnetosonic Mach number) in the plasma.

In the case of magnetized planets the obstacle to the solar wind is the planetary magnetic field. The outer limit of the planet's field of influence is known as the "magnetopause". The volume within, which the planet's field dominates, is the "magnetosphere". The size of the magnetosphere is governed by the relative strengths of the magnetic field and the solar wind pressure at the planet. Planets with strong intrinsic magnetic field, such as Earth, Jupiter and Saturn, have large and complex magnetospheres. The magnetospheres of these planets differ both in size and internal energy sources but also in the strength of the solar wind flow past them. Thus, the interaction of each of the magnetospheres with the solar wind differs in some degree from the others. Russell (1991) reviewed the basic physical processes that occur in those magnetospheres, and briefly highlighted our exploration of these planets and the problems remaining. The terrestrial magnetosphere is of course the one that has been most thoroughly studied, but given the recent Gallio and Cassini missions, we now also have

significant information on Jupiter and Saturn's magnetospheres. This type of interaction will not be discussed in this chapter any further, as there exists a very extensive literature on this subject, including books, book chapters and review articles (e.g. Cravens 1997a; Dessler 1983; Khurana 2004)

In the case of a planet without a global magnetic field, like Mars and Venus, the standing bow shock location is much closer to the obstacle body, and the shocked solar wind interacts directly with the ionosphere and the upper atmosphere of the planet (e.g. Nagy et al. 2004; Russell et al. 2007). Many of the planetary satellites and asteroids are either exposed directly to the solar wind or to the planet's magnetospheric plasma, because they have small or no intrinsic magnetic fields and possess no significant atmospheres. However, some of the satellites such as Saturn's largest moon Titan, for example, and some comets (when close enough to the Sun), do have a substantial atmosphere and thus an ionosphere, and possess no or only small intrinsic magnetic fields. The interaction of these non-magnetic objects with the planet's magnetospheric plasma or the solar wind is expected to be similar to the solar wind interaction with Mars and Venus.

1.2 The Potential Importance of the Ionosphere/Atmosphere System

At planets and moons that have an atmosphere, the neutral atoms and molecules may be photo-ionized by sunlight (or starlight, in the case of extra-solar planets) or by the impact of energetic particles. In some cases, the degree of ionization may reach 10^{-6} or even 10^{-5}, generating a region in the atmosphere that is known as the ionosphere. The resulting situation is one in which, at altitudes that usually correspond to the thermosphere, ions and electrons coexist with the much more abundant neutral atmosphere.

The ionosphere/atmosphere system is especially important to understand the plasma interaction around non-magnetic solar bodies. Without the shielding of a strong intrinsic magnetic field, the upstream plasma can easily come close to the body, thus interact more directly with the neutral atmosphere/ionosphere. The interaction of the inflowing plasma with the ionosphere/atmosphere system is through electro-magnetic forces and collisions.

This chapter will discuss in details the plasma interaction with the ionosphere/atmosphere system. The chapter is organized as follows. The next section discusses plasma flow interaction with un-magnetized planets: Venus and Mars. Plasma interactions around satellites and comets are discussed in Sects. 3 and 4, respectively. Section 5 provides a brief discussion of the coupling between an ionosphere and magnetosphere for magnetized planets. A few brief comments are given in the last section.

2 Un-magnetized Planets: Venus and Mars

Venus and Mars are non-magnetized or weakly magnetized inner planets with substantial atmospheres and ionospheres. As a consequence, the plasma environments around these two bodies are similar in many ways.

2.1 Venus; General Interaction Features

Many spacecraft flew by, orbited, probed or landed on Venus. However, our present understanding of the solar wind interaction with Venus primarily comes from observations made during the Pioneer-Venus Orbiter (PVO) mission, which lasted 14 years, had a broad and relevant instrument payload and covered more than an entire solar cycle (Russell et al. 2006).

PVO observations of Venus plasma environment and upper atmosphere are reviewed in several comprehensive volumes (J. Geophys Res., **85**, A13, 1980; Space Sci., Rev., **55**, 1991) and two books Venus I and Venus II by the University of Arizona Press. In addition the literature through the 1990s contains the descriptions of many individual in-depth analyses. Two recent reviews by Russell et al. (2006, 2007) have also been published. The reader is encouraged to explore beyond the short list of references provided here. The recently launched Venus Express spacecraft (Titov et al. 2006), equipped with a magnetometer (Zhang et al. 2006) and a comprehensive plasma instrument package with an ion mass analyzer, an electron spectrometer and energetic neutral atom (ENA) images (Barabash et al. 2007a, 2007b) is now also adding new, important and complimentary information on the Venus plasma environment.

The observations by Venera 9, 10 and PVO spacecraft showed that Venus has no intrinsic dipole magnetic field (Dolginov et al. 1978; Yeroshenko 1979; Russell et al. 1980). Figure 1 illustrates the major features of the solar wind interaction with Venus's ionosphere deduced from the solar maximum measurements obtained by PVO. The most basic features are the bow shock that defines the outer boundary of the interaction, followed by the large-scale draping of the interplanetary magnetic field over the ionosphere in the magnetosheath and the related comet-like "induced magnetotail" made up of the innermost draped flux tubes that have been slowed where they pass through the upper atmosphere and ionosphere.

The solar cycle causes changes in the effective obstacle presented by Venus to the solar wind. Figure 2, from Phillips and McComas (1991), illustrates the reduction in the termi-

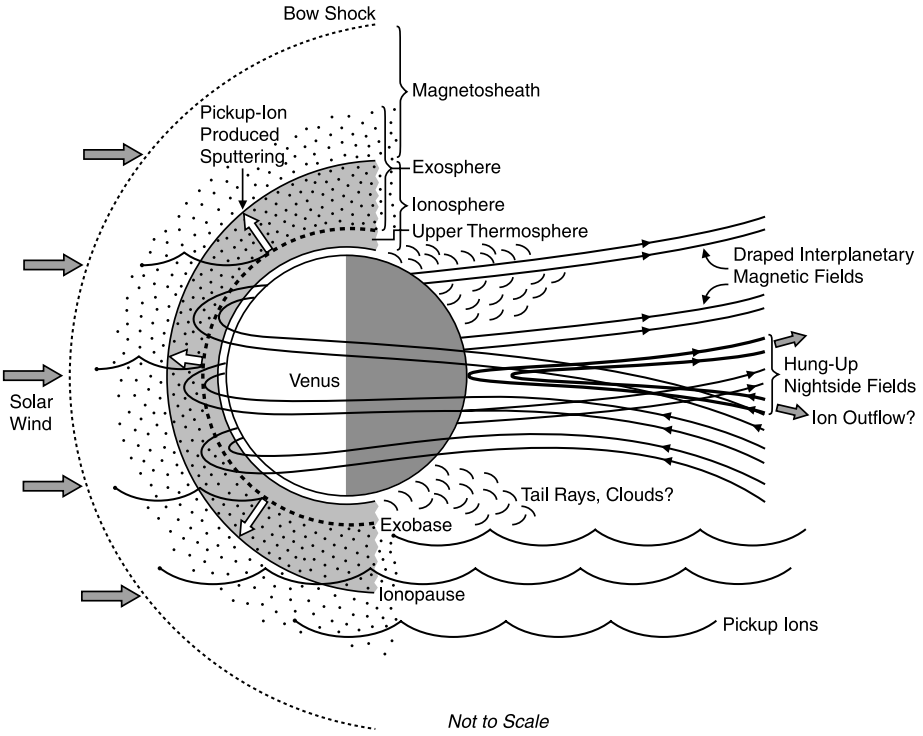

Fig. 1 Schematic diagram of the solar wind interaction with Venus, including the oxygen escape processes (Russell et al. 2007)

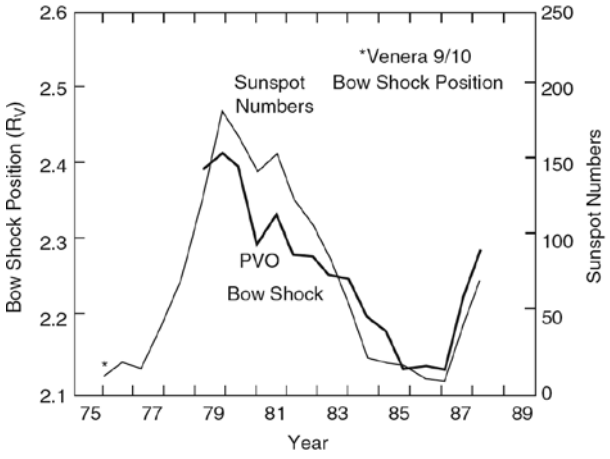

Fig. 2 Location of the bow shock, normalized to the terminator, measured by PVO through 1987 (*heavy trace*). *Light trace* shows the sunspot number averaged over each PVO observing season of roughly 100 Earth days. The asterisk at lower left marks the bow shock location observed by Venera 9 and 10 (Phillips and McComas 1991)

nator location of the bow shock with solar EUV flux, implying that the obstacle has either become smaller or is no longer impenetrable (Zhang et al. 1991a, 1991b). The shape of the shock can be fit quite well with a simple conic function: $r = R_T/(1 + \varepsilon\cos(\chi))$, where r is the radial distance to the shock, χ is the Sun–Venus–satellite angle and R_T is the radius of the terminator shock (Russell 1977). Slavin et al. (1980) found that the best fit to the observed PVO bow shock crossing corresponds to an ε of 0.88 and an R_T of 2.21 R_V. Venus Express has obtained 147 clear crossings from April to August 2006 (Zhang et al. 2007). The best fit to the bow-shock location from a solar-zenith angle of 20° to 120° gives a terminator bow-shock location of 2.14 R_V, and subsolar bow shock at 1.32 R_V, about 1,900 km above the surface of the planet. Statistical studies also showed that the location of the Venus bow shock is not only dependent on the solar cycle and solar EUV flux, but is also tightly related to the upstream solar wind parameters, including the orientation of the interplanetary magnetic field (Russell et al. 1988; Zhang et al. 1991a).

Signatures of the Venus obstacle have also been seen upstream of the bow shock in the high resolution PVO magnetic field data and as well as in the plasma wave data (Crawford et al. 1993). Some of the solar wind protons and electrons incident on the nose of the bow shock are accelerated back into the oncoming solar wind along interplanetary magnetic field lines as they connect to the shock. This phenomenon produces the foreshock, a feature observed as upstream magnetic field and plasma fluctuations, and plasma waves, in front of virtually every planetary bow shock encountered in the solar system. The magnetic field and plasma fluctuations associated with the foreshock can be convected with the solar wind into the magnetosheath where they produce turbulent conditions on magnetosheath streamlines connected to the portion of the shock downstream from the foreshock (Luhmann et al. 1983). These fluctuations may affect the ion pickup process, discussed below, in the magnetosheath.

In the subsolar magnetosheath the magnetic field lines "pile up" and close to the top of the ionosphere form a magnetic barrier. Features of this magnetic pile-up region (MPR) near Venus are rather well established, because the PVO crossed this region hundreds of time (Zhang et al. 1991b). The peak pressure of the IMF measured within the MPR is typically about 83% of that of the upstream solar wind value and is balanced by the ionospheric thermal pressure. The mean distance between the topside boundary of the ionosphere, the ionopause, and the surface where the IMF pressure reaches 50% of the local dynamic pres-

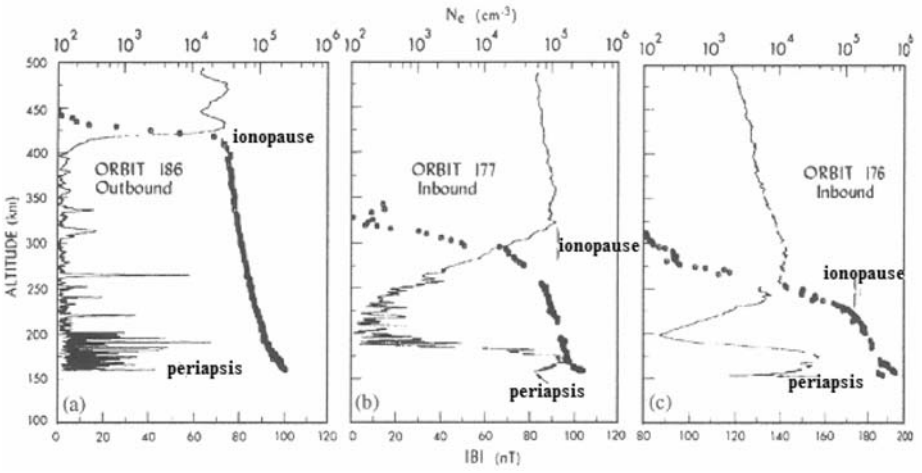

Fig. 3 The altitude profile of the magnetic field strength and the plasma density in the Venusian ionosphere in period of low (orbit 186), moderate (orbit 177) and high (orbit 176) dynamic pressure of the SW (from Elphic et al. 1981)

sure of the solar wind is about 200 km at the subsolar point and 800 km at the terminator. The peak IMF pressure decreases from the subsolar point to the terminator approximately following a $\cos^2\theta$ law (θ is the solar zenith angle). The so called ionopause is the location of the transition from magnetic to ionospheric thermal pressure. The ionopause has been identified by Brace et al. (1980) and Knudsen et al. (1980) as the altitude where the thermal plasma density is approximately equal 100 cm^{-3}. Cloutier et al. (1983) defined the ionopause simply as a drastic change in the plasma density. Phillips et al. (1984) used a definition of the ionopause as the point at which the magnetic and thermal pressure crossed upon entry or exit from the ionosphere.

Figure 3 shows examples of ionopause measured by PVO. The left figure, Orbit 186, represents condition when the ionospheric thermal pressure well exceeds the solar wind dynamic pressure and the transition region is above the collisional region of the ionosphere, resulting in a sharp ionopause. Under these conditions the magnetic barrier magnetic field is essentially excluded from the ionosphere by currents flowing in the ionopause layer (Elphic et al. 1981; Luhmann and Cravens 1991). The two plots on the right hand side of Fig. 3, corresponding to Orbits 177 and 176, show what happens when the solar wind pressure increases and pushes the pressure balance altitude into the collisional region of the ionosphere. This situation can arise either because of very high solar wind pressures, mostly during solar cycle maximum, and/or reduced ionospheric pressure conditions. Under these circumstances the magnetic field penetrates the ionosphere resulting in magnetic field strength in excess of 100 nT. This is accompanied by a "thick" ionopause. These observations have been successfully modeled by Shinagawa and Cravens (1988) using a one-dimensional multi-fluid MHD model as being due to downward convection into the ionosphere due to both magnetic pressure and aeronomically controlled pressure gradients combined with ohmic dissipation near 150 km.

Solar wind dynamic pressure at Venus varies according to a distribution dictated mostly by solar conditions. For the period of PVO observations of the ionosphere, the overall spread and occurrence frequency of values obtained from the Plasma Analyzer is given in Fig. 4 (Phillips et al. 1984). Even at solar maximum, the number of times the solar wind pres-

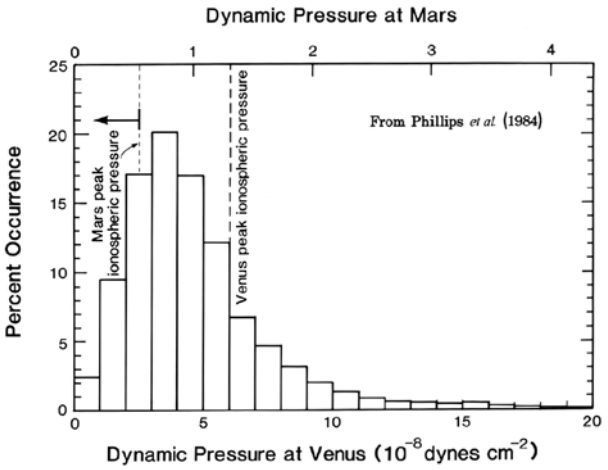

Fig. 4 Histogram of solar wind dynamic pressure at Mars and Venus. Dashed lines are peak effective ionospheric thermal pressure (from Phillips et al. 1984)

sure exceeds the peak thermal pressure of the ionosphere, a measure of its robustness as an obstacle, is small relative to the situation inferred for Mars. The related solar zenith angle dependence of the ionopause altitude determined from both the topside ionosphere density gradients and the altitudes where ionospheric thermal and magnetic barrier magnetic pressures balance is shown in Fig. 5a. As the solar wind pressure increases the height of the ionopause decreases and actually levels of near 300 km, when the pressure exceeds about 4×10^8 dyn cm^{-2}. The observations also showed that the mean ionopause height increases from about 350 km at the subsolar point to about 900 km at the terminator (see Fig. 5b). The observed ionopause altitude behavior follows a roughly cosine solar zenith angle squared dependence because the component of the dynamic pressure normal to the boundary is the one that is important for the pressure balance. It is also much more variable at high solar zenith angles than low, in part because of the cosine squared dependence but also because attached structures such as ionospheric clouds and tail rays are often observed at the ionopause there. In addition Phillips et al. (1988) showed that the ionopause has an elliptical cross section at the terminator, with generally higher altitudes found at the poles of the magnetosheath field draping pattern.

2.2 Atmosphere Escape from Venus

The typical altitude of pressure balance with the Venus ionosphere, and in the absence of balance, the altitude at which the transition from solar wind to the ionospheric plasma occurs, is such that the exosphere is exposed to the solar wind plasma and/or magnetic field. In addition, the ionospheric chemistry is such that the dissociative recombination reaction of O_2^+ results in pairs of suprathermal oxygen atoms populating the exosphere; there is also a significant hydrogen exosphere present (Nagy and Cravens 1998; Kim et al. 1998; Hodges 2000). Any ionization mechanism that operates in these upper regions of the neutral atmosphere, including photoionization, charge exchange with solar wind protons, or electron impact by solar wind electrons, produces a seed population for the ion pickup process. Ion pickup, illustrated by Fig. 6, can lead to either atmosphere escape or to impact of the pickup ion on the atmosphere, with energy deposition and possible sputtering loss of additional atmosphere (Luhmann and Kozyra 1991). The signature large cycloidal trajectories of Venus O^+ pickup ions suggested in Fig. 6 are

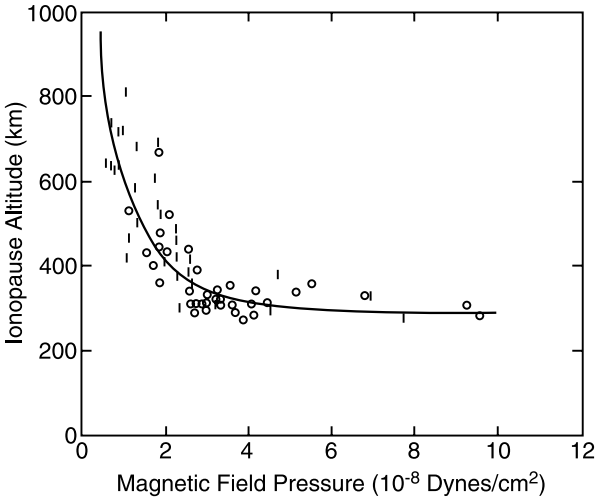

Fig. 5a The response to the ionopause altitude, inbound (I) and outbound (O), to the orbit to orbit changes in magnetic pressure. The ionopause altitude declines with increasing solar wind pressure, but levels above about 4×10^{-8} dyn cm^{-2} (Brace et al. 1980)

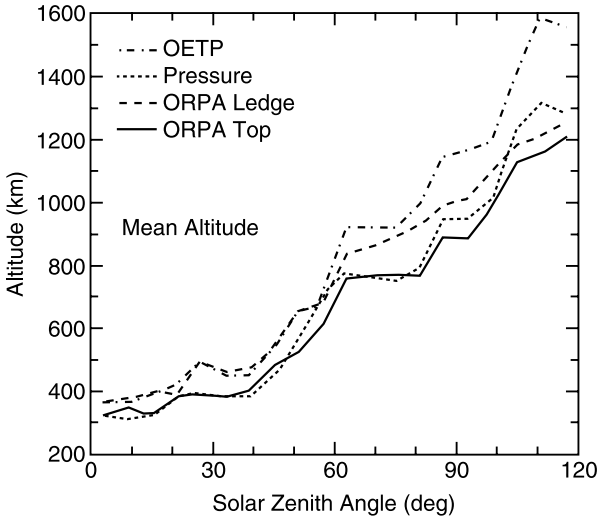

Fig. 5b The solar zenith angle variations of the ionopause height using ionopause definitions based on various PVO measurements. All definitions show similar SZA variation of the ionopause height (Phillips et al. 1988)

most relevant for high altitude pickup of the atomic oxygen coronal atoms. Smaller cycloids and helices are expected for smaller mass hydrogen pickup, and for O^+ picked up in the slowed background plasma flows and stronger, draped magnetic fields in the Venus magnetic barrier region where most of the pickup must occur. The suprathermal oxygen ions observed on PVO at the top of the dayside ionosphere (Kasprzak and Niemann 1982; Grebowsky et al. 1993) and in the low altitude wake (Kasprzak et al. 1991) are likely evidence of this population.

An ongoing debate concerns the importance of this mechanism for atmosphere evolution at Venus, as for Mars (see Russell et al. 2007). At Venus, however, the gravitational field is such that pickup is one of the only ways that oxygen can be lost to space. Venus is notoriously dry compared to Earth, and while it is easy to envision the hydrogen from photodissociated water vapor in the upper atmosphere escaping, oxygen should be retained.

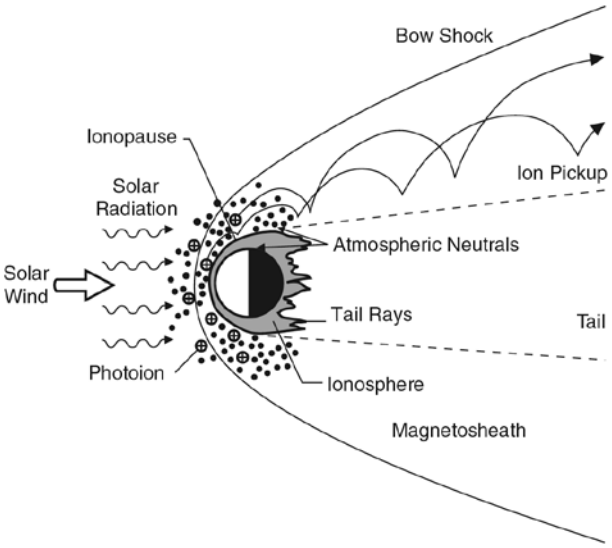

Fig. 6 Schematic illustration of the pickup of heavy planetary ionospheric ions at Venus and Mars. Only those ions produced in the region where the solar wind plasma flows are removed. They are either carried away with the solar wind or "precipitate" into the lower atmosphere, depending on the location where they are produced and the direction of the interplanetary magnetic field (Luhmann and Kozyra 1991)

Over time, this oxygen would have had to be removed from the atmosphere by some process such as oxidation of the surface. But if Venus originally had an Earth-like inventory of water, it would be difficult for the crust to have accommodated this amount. Thus escape to space by ion pickup and associated sputtering is a viable candidate for further examination. This historical aspect, as well as an understanding of the present-day Venus-solar wind interaction consequences, has motivated several special analyses of the PVO data.

The average indirectly inferred escape rates from PVO observations, of the order of 5×10^{24} $\sec^{-1}$ (McComas et al. 1986), fall far short of those needed to remove an ocean's worth of oxygen. However, conditions for this process to be effective may have been more favorable in the past. In particular, periods of disturbed solar wind from coronal eruptions and stream interactions have been found to enhance lower energy oxygen ion escape, as observed by the PVO Neutral Mass Spectrometer (Luhmann et al. 2007). Observations of ion escape by the ASPERA-4 experiment on Venus Express (Barabash et al. 2007a, 2007b) are well suited to measure the ion escape rates from Venus. Preliminary observations indicate an escape rate in the order of 10^{25} $\sec^{-1}$.

Several "bulk removal" processes for ion loss have also been suggested based on the PVO observations. These observations include the "clouds", attached and detached regions of ionospheric plasma detected above the nominal ionopause, as shown in the Langmuir Probe time series, and "tail rays" of thermal electrons and ions detected in the near-Venus wake (see Brace et al. 1995). The clouds were analyzed by Ong et al. (1991) and found to be associated with interplanetary field rotations, suggesting they may be transient features such as ridges on the ionopause, associated with changing interplanetary field draping. Hybrid model calculations by Terada et al. (2002) also indicate that Kelvin–Helmholtz instabilities at the ionopause result in filaments/streamers that can move down the tail and escape.

2.3 Mars

The data from the Phobos 2 mission created two, controversial hypotheses: one stated that Mars has a substantial intrinsic magnetic moment ($\sim 1.4 \times 10^{22}$ G cm^3, Dolginov and Zhuzgov 1991) and while the other claimed that the intrinsic magnetic field of Mars is negligible

(Yeroshenko et al. 1990). This controversy was settled by magnetometer (MAG/ER) carried by the Mars Global Surveyor (MGS) which clearly established the presence of intense crustal magnetic anomalies and set an upper bound of 2×10^{17} A m^2 $= 2 \times 10^{20}$ G cm^3 on the intrinsic dipole field at Mars (Acuna et al. 1998, 1999; Connerney et al. 1999; Ness et al. 1999). This corresponds to an equatorial surface field of less than 0.5 nT. The magnetic fields measured by the MGS magnetometer over certain localized regions were found to range up to 1600 nT. Such fields are sufficiently strong to withstand the solar wind pressure up to near 400 km. The crustal sources are distributed mainly over the surface of the southern hemisphere with the largest concentration in the geographic range of 120–210°W and 30–85°S. These anomalies complicate at least locally the plasma environment of Mars.

2.3.1 The Size, Shape and Variability of the Bowshock (BS) at Mars

The location of the bow shock at Mars is more distant and also more variable than for Venus: in the terminator plane, 2.66 R_M versus 2.39 R_V with a standard deviation of 0.49 R_M versus 0.21 R_V during solar maximum, based on Phobos 2 observations (Slavin et al. 1991). The MGS results showed that, during periods of medium solar activity, the terminator distance of the shock is at 2.62 R_M with a standard deviation of 0.33 R_M. Also note that the sunspot number was 140–180 and 30–90 respectively, for the Phobos 2 and MGS missions, so this also suggests that the mean Martian BS position is independent of the solar cycle and EUV flux. This is different from Venus as discussed in the previous section.

Trotignon et al. (2006) recently reanalyzed a total of 700 shock crossings, using the mixed data set of Phobos 2 and MGS. As shown in Fig. 7, the shock locations are highly variable. The best fit corresponds to a subsolar shock location at 1.63 ± 0.1 R_M, these results are consistent with previous studies (Vignes et al. 2000)

Several factors that control the Martian shock locations were examined by Vignes et al. (2002) based on 553 MGS shock crossings. Contrary to many expectations, the high crustal magnetic sources, found in the southern hemisphere, do not seem responsible for the bow shock (BS) variability. Data results show no obvious strong correlation between the location of the highest crustal sources and the variability of the shock position. However, a recent study by Edberg et al. (2008) found that the shock locations are further away from the planet when the crossing was observed over regions with strong crustal fields. The new results are

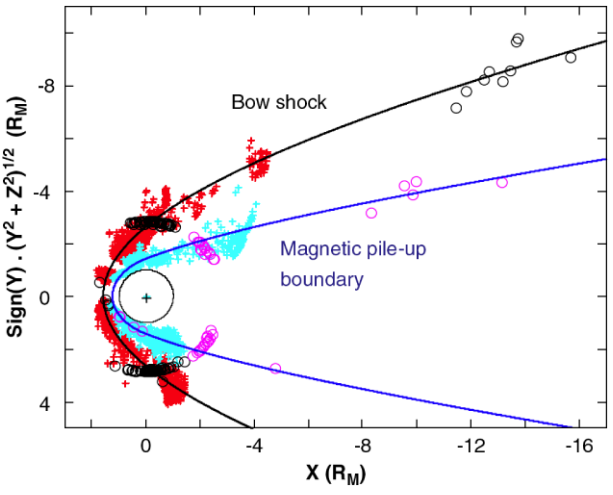

Fig. 7 Martian bow shock (*black line*) and magnetic pileup boundary (*blue line*) models that best fit to the observations made by both the plasma wave system of the Phobos 2 mission (*black rings* for the BS and *purple rings* for the MPB) and the MAG/ER MGS (*red crosses* for the BS and *blue crosses* for the MPB). (Trotignon et al. 2006)

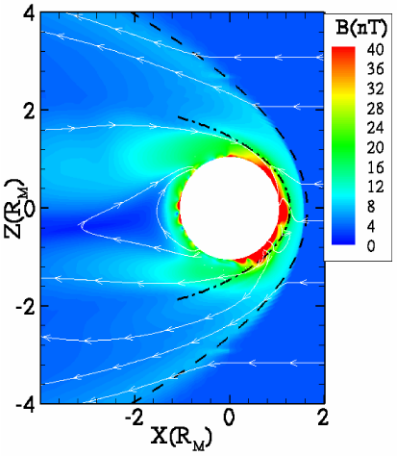

Fig. 8 The calculated magnetic field in the meridianal plane. The *color plots* show the magnitudes; the *white lines* marked with arrows indicate the vector direction of the magnetic field. The *dashed line* represents the mean bow shock and the *dash-dot line* is the mean MPB locations from Vignes et al. (2000) (Ma et al. 2004)

also consistent with the global multi-species MHD model results of Ma et al. (2002), which found that the crustal sources do move the shock boundary outward significantly. Numerous complex 3-D models have been developed during the last decade to model solar wind interaction with Mars. These models are either based on MHD formulations (e.g. Ma et al. 2004; Harnett and Winglee 2006; Ma and Nagy 2007) or hybrid formulations (e.g. Kallio and Janhunen 2002; Bösswetter et al. 2004; Modolo et al. 2005). Both of these approaches have advantages and disadvantages as discussed in an accompanying paper/chapter by Ledvina et al. (2008) and in some respect complement each other. These models have been successful in reproducing the observed bow shock and magnetic pile-up locations rather well. An example of such successful model and observation comparison is shown in Fig. 8, from the work of Ma et al. (2004).

Vignes et al. (2002) also found that when the classical definitions of quasi-parallel ($\theta_{Bn} \leq 45°$) and quasi-perpendicular ($45° \leq \theta_{Bn} \leq 90°$) shocks are used, the mean value of the terminator distance for the quasi-parallel shock crossings is about 3% closer than for the quasi-perpendicular shock crossings. This creates a dawn–dusk asymmetry in the bow shock location, because according to the IMF orientation, quasi-parallel shocks dominate the dawn side while quasi-perpendicular shocks dominate the dusk side. This asymmetry is consistent with a previous study on Venus and Mars (Zhang et al. 1991a), which found the quasi-parallel shock is closer to the planet than the quasi-perpendicular shock. Similar to Venus, the Martian shock also appears farther from Mars in the hemisphere of the locally upward interplanetary electric field (Vignes et al. 2002), which is consistent with the idea that mass loading plays a role in controlling the bow shock location,

In summary, the shock position at Mars is observed to be different than that of Venus. Although the shock location around Mars is found to be highly variable, according to the statistical study, the shock location has only a slight dawn–dusk asymmetry depending on the IMF direction, small dependence on the convection electric field direction, no significant effect due to solar cycle conditions, while the effect of crustal sources is still under debate. Although there is no direct solar wind pressure data for the shock crossings, we can expect that the solar wind dynamic pressure will also contribute to the variations of Martian shock location, as is the case for Venus.

2.3.2 *Magnetic Pile up Region and Magnetic Pileup Boundary (MPB) Characteristics*

The magnetic pileup boundary (MPB) is a sharp, thin, and well-defined plasma boundary located between the bow shock and the upper ionosphere boundary at Mars (Fig. 9). This boundary separates the magnetosheath, a region of low magnetic fields with significant wave activity, from the magnetic pileup region dominated by strong, highly organized magnetic fields, which are a result of the pileup and draping of the interplanetary magnetic field.

The MPB appears in the MAG/ER data as a layer in which the measured magnetic fields increase over a short radial distance (Vignes et al. 2000). Simultaneously, the electron fluxes measured by the electron reflectometer (ER) attenuate in a manner consistent with electron impact ionization of the oxygen and hydrogen exosphere by solar wind electrons (Crider et al. 2000). Coincident with this location, wave activity in the MAG data declines with decreasing altitude. Previously, instruments onboard Phobos-2 detected a boundary consistent with the MPB location when comparing the respective fits (Trotignon et al. 1996; Vignes et al. 2000). The Phobos-2 instruments, ASPERA (Lundin et al. 1989) and TAUS

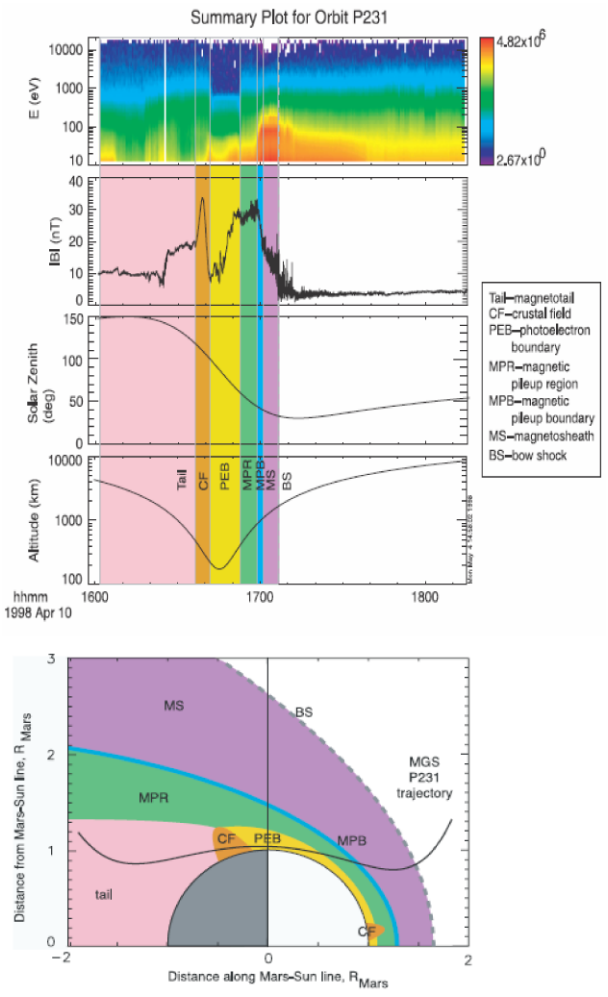

Fig. 9 Magnetic pile-up boundary (MPB) detected at MGS in the Martian magnetosheath (*left*) and cylindrical projection of the trajectory of MGS to show the locations of the different regimes of plasma regions at Mars (Crider et al. 2003)

(Rosenbauer et al. 1989) saw the MPB (then called "planetopause") as a termination in solar wind proton flux in the same location as the magnetometers sensed an increase in magnetic field values (Riedler et al. 1989). These attributes indicate that solar wind protons are interacting through charge exchange with the planetary exosphere. If one puts this together with the complementary MGS observations of electron impact ionization and wave activity then the MPB appears to be the transition to the region in which the planetary exosphere becomes substantial in determining the plasma properties. A complete discussion on the Martian MPB based on MGS and Phobos 2 measurements is given by Nagy et al. (2004).

It is important to note that the MPB is neither a pressure balance boundary nor a discontinuity in the solar wind flow. ER data show the presence of solar wind electrons everywhere above the photoelectron boundary (Mitchell et al. 2000). Therefore, the solar wind plasma and magnetic field do penetrate the MPB. The MPB simply marks the transition from shocked solar wind plasma to plasma that is interacting and/or has interacted with the exosphere.

Recently, new features were discovered which indicated that the MPB is a boundary of the induced magnetosphere. Bertucci et al. (2003) found a strong and sudden enhancement of the magnetic field draping at the MPB of Mars, in contrast with the picture of a gradual draping between the bow shock and the final planetary obstacle. The boundary marks then the entrance into an induced magnetosphere, where draping is strong. In this region, the magnetic field lines frozen into the electron gas follow the denser and cooler plasma. This is a consequence of the mass loading and ionization mechanisms, which contribute to the dominance of heavy ions of exospheric origin (Lundin et al. 1990; Crider et al. 2000). The lower limit of this region is the final planetary obstacle (Luhmann 1986; Mitchell et al. 2001). These results are highly consistent with Phobos 2 observations across the magnetic tail boundary at 2.86 R_M (Yeroshenko et al. 1990).

2.3.3 The Ionopause at Mars

The ionopause is a feature almost always observed in the ionosphere of Venus by radio occultation and in-situ instruments onboard the Pioneer Venus Orbiter (Kliore 1992; Brace and Kliore 1991). The ionopause is marked by sharp decrease in the electron density at the top of the ionosphere as discussed in the previous section. However, no clear ionopause signatures at Mars have been reported so far. A boundary between the Magnetic Pileup Region and the ionosphere below is evident in the supra-thermal electron observations (>10 eV) by MGS. This boundary has been called the "photoelectron boundary" (Crider et al. 2003; Nagy et al. 2004). However, it is not clear at all how this transition is related to the classical ionopause. Both the Mars Express radio occultation and radar data seem to give hints of thermal electron density transitions, but so far no definitive results have been published. It has long been known from Viking measurements, that the ionospheric thermal pressure at Mars is usually insufficient to balance the total pressure in the overlying Magnetic Pileup Region (see Fig. 4). Thus, it is expected that the Martian ionosphere is magnetized, much like Venus' ionosphere during times of high solar wind dynamic pressure and/or low solar cycle conditions. It was found at Venus that under such conditions the ionopause is not a sharp feature. The magnetic pressure associated with this ionospheric field will supplement the ionospheric thermal pressure, possibly enough to balance the overlying MPR pressure. Crustal magnetic fields vastly complicate the topology of the ionosphere and thus conditions for the formation of a "classical" ionopause.

2.3.4 Atmosphere Escape from Mars

The gravity at Mars is significantly lower than it is at Venus thus more processes can contribute to the escape flux. Some of the neutral oxygen atoms created from the dissociative recombination of O_2^+ ions have enough energy to escape. This process is considered to be the main contributor to the escape of neutral oxygen atoms, although charge exchange with hot H^+ and O^+ ions can also make a contribution. The estimates of the neutral oxygen escape flux vary widely from about 2×10^{26} to 1×10^{25} sec^{-1} (Kim et al. 1998; Hodges 2002; Chaufray et al. 2007). Ma and Nagy (2007), using a 3-D MHD model estimated that the escape flux of ionospheric and pick up ions varies between about 3×10^{24} to 3×10^{23} sec^{-1} under "normal" solar cycle maximum and minimum conditions. Chaufray et al. (2007) using a comprehensive, combined hybrid and precipitation models find that the pick up ion, ENA and sputtered escape fluxes are in the range of 2×10^{23}–3×10^{24}, 4×10^{22}–4×10^{23} and 2×10^{23}–7×10^{23} sec^{-1} respectively. The Mars Express ASPERA instrument measured the escape flux of ions in excess of about 30 eV; they estimated a total flux of about 3.2×10^{23} sec^{-1} during solar minimum (Barabash et al. 2007a, 2007b).

3 Satellites

As discussed before, satellites with an atmosphere can interact with the corotational plasma flow inside a planetary magnetosphere. As a consequence, the corotational plasma near the moon will be disturbed. This section focuses on plasma flow interactions around several Galliean satellites and Titan, the largest moon of Saturn.

3.1 Galilean Satellites

Each of the Galilean satellites of Jupiter has a tenuous atmosphere by terrestrial standards. In the discussion below, supporting references may be found in the book chapter by McGrath et al. (2004). Io is unique in the solar system with an SO_2 atmosphere that is ultimately derived from continual volcanic eruptions, either directly injected into the atmosphere or indirectly via deposition on its surface and subsequent sublimation. Normally, Io's atmosphere is most abundant at lower latitudes where most of the volcanic activity occurs. In the southern polar region the atmosphere almost becomes an exosphere, and also in the northern polar region when the large volcano Tvastar is inactive. The atmosphere is longitudinally asymmetric with higher densities in the trailing and anti-Jupiter quadrant. Accordingly, it is characterized by spatial and temporal variability. Besides SO_2, the other driving gas for volcanoes is S_2, which has a short chemical lifetime in the atmosphere and hence a minor constituent. Other detected gases in the atmosphere include SO, O, S, NaCl, Na, K, as listed in Table 1. SO and NaCl are thermochemical components of hot volcanic gaseous plumes. Photochemistry combined with the magnetospheric interaction with the atmosphere yields SO, O, S, Na, and K. At the equator the surface pressure is about 1 nbar. The canonical mass loss rate from Io is $\sim 2 \times 10^{30}$ amu sec^{-1} and mostly neutrals, rather than ions. This implies that the residence time or lifetime of the atmosphere is a mere 3 days and must be continually re-supplied on a time scale less than a week.

The magnetospheric interaction with Io's atmosphere produces a substantial ionosphere with electron densities as large as 3×10^5 cm^{-3}. The electron densities are organized with respect to the ram direction rather than the subsolar point (Hinson et al. 1998). The highest densities are found on the flanks and the lowest in upstream and downstream directions

Table 1 General properties of the Galilean satellites' atmospheres, ionospheres, and magnetospheric interaction[a]

Quantity	IO	Europa	Ganymede	Callisto
Atmospheric source	Volcanoes	Sputtering H_2O ice	Sputtering H_2O ice	Sputtering H_2O ice
$P_{surface}$ (nanobar)	1	0.0007	0.0007	0.008–0.3
Column density (cm^{-2})	3×10^{16} $(0.03–10) \times 10^{16}$	5×10^{14} $(3–7) \times 10^{14}$	5×10^{14} $(1–10) \times 10^{14}$	8×10^{14} CO_2 $\sim 3 \times 10^{16}$ O_2
Major gas	SO_2	O_2	O_2	O_2 or CO_2?
Other species	S_2, SO, O, S, NaCl, Na, K	O, H_2O, H_2, H, Na, K	O, H_2O, H_2, H	CO_2, O, H_2O, H_2, H, CO, C
Thermospheric temperature (K)	~2000	~2000	~1000	~2000
Escape rate (s^{-1})	1.6×10^{28} SO_2	5×10^{26} O_2	?	?
Lifetime (d)	3	4	?	?
Peak electron density (cm^{-3})	$\sim 3 \times 10^5$	$\sim 10^4$	$< 10^3$	$\sim 2 \times 10^4$
Σ_P (mho)	~100 (ec)	~14	≤100 (pu)	$\sim 10^4$ (ec)
Σ_H (mho)	~150 (ec)	~10	≤100 (pu)	$\sim 10^4$ (ec)
Σ_A (mho)	5	1.7	2	1.3
$V_{rel\ plasma}$ ($km\ s^{-1}$)	57	90	180	170
V_{alfven} ($km\ s^{-1}$)	220	460	375	600
M_A	0.25	0.2	0.5	0.3
M_S	1.65	1.75	2.4	2.4
B (nT)	1800, J	420, J	750, G	35, J
E_0 ($V\ m^{-1}$)	0.1	0.04	0.02	0.006
$\alpha = E_i/E_0$	0.1	0.2	–	0.001
I_{iono} (10^6 A)	10	1.4	–	0.15
Joule heating (W)	4×10^{11}	3×10^{10}	?	$\leq 10^9$
$\lvert \Delta B/B_J \rvert$	0.45	0.4	–	0.35
Magnetospheric ion power (W)	2×10^9	1×10^8	$\sim 10^7$	$\sim 10^4$
Solar EUV/UV power input (W)	7×10^9	$< 10^8$	$< 10^8$	5×10^7, CO_2

ec = elastic collisions, pu = pickup, J = Jupiter's magnetic field, G = Ganymede's magnetic field

[a]Adopted from Strobel (2005)

with a downstream wake or tail consistent with acceleration of plasma up to local corotation speed. There is no evidence that Io possesses either an intrinsic or an induced magnetic field that exceeds the local Jovian magnetic field strength above the surface.

Europa and Ganymede have atmospheres produced by ion sputtering of the water ice surfaces, comprised mostly of O_2, with approximately picobar surface pressures (Johnson 1990). Whereas the sputtering yield of H_2O molecules is about 7 times larger than the O_2 yield, H_2O molecules stick on every collision with the cold surface, whereas the O_2 sticking coefficient is much lower (~0.001) and hence O_2 emerges as the dominant atmospheric con-

stituent. Other products of ion sputtering such as H, H_2, O, and OH escape the weak gravitational field of these satellites, especially H and H_2. For Europa, Smyth and Marconi (2006) estimate an escape rate of 2×10^{27} H_2 s^{-1}, which creates a gas torus. These O_2 atmospheres have column densities in the range of (1–10) $\times$ 10^{14} cm^{-2}. Europa's O_2 atmosphere escapes by magnetospheric interaction with a rate $\sim 5 \times 10^{26}$ O_2 s^{-1} leading to a short lifetime of $\sim$2 days. A big difference between Europa and Ganymede is the extent of their ionospheres and the fact the Ganymede has an intrinsic magnetic field, while Europa has an induced magnetic field presumably from a conducting ocean below the surface moving through the strong Jovian magnetic field. Peak electron densities on Europa reach $\sim 10^4$ cm^{-3} (Kliore et al. 1997), whereas on Ganymede an ionosphere is only marginally detectable with at most densities of $\leq 10^3$ cm^{-3} in the equatorial regions. However for Ganymede, other estimates are available based on interpretation of HST UV auroral observations by Eviatar et al. (2001). It is highly probable that the electron density could reach $\sim 10^5$ cm^{-3}, along the auroral ovals located at the separatrix between Ganymede's intrinsic magnetic field and the Jovian magnetic field. Note that these latitudes were not probed by Galileo radio occultations.

For Callisto, Carlson (1999) provided a direct measurement of the CO_2, using near-IR bright limb emission and inferred a vertical column density of 8×10^{14} cm^{-2}, whereas Kliore et al. (2002) inferred from radio occultation measurements of the electron density that another, larger component must be present in the atmosphere to explain electron densities of $\sim 10^4$ cm^{-3}. They suggested neutral column densities on the order of 3×10^{16} cm^{-2}, most probably O_2 by analogy with Europa and Ganymede. Thus the surface pressure is at most $\sim$0.3 nbars. Of particular importance, Kliore et al. (2002) concluded that a necessary condition to have an ionosphere is that the trailing hemisphere be partially solar illuminated.

For Io and Europa, the harsh environment of Jupiter's inner magnetosphere produces atmospheric chemistry driven by magnetospheric electrons as well as by solar radiation. In fact, electron impact dominates atmospheric ionization and UV emission. With the much lower magnetospheric electron densities at the orbits of Ganymede and Callisto, solar photoionization exceeds electron impact ionization.

With observations available for neutral and electron densities specifically measured ionospheric electron density profiles, ($\sim 10^4$–10^5 cm^{-3}) for Io, Europa, and Callisto, it is straightforward, with a reasonable assumption about the main ion's mass, to compute Pedersen (Σ_P) and Hall (Σ_H) conductances and compare them with the Alfven conductance (Σ_A). Typical values are given in Table 1. The ionospheric Pedersen and Hall conductances in all cases substantially exceed the respective Alfven conductances. For satellite electrodynamic interactions, other relevant quantities include the velocity of magnetospheric plasma relative to the satellite, $V_{\text{rel plasma}}$, the Alfven velocity, V_{alfven}, the Alfven Mach number, M_A, the sound speed Mach number, M_S, the magnetic field strength, B, and the corotation electric field, E_0. The strength of the electrodynamic interactions of the Galilean satellites with the Io plasma torus (plasma in Jupiter's inner magnetosphere) can be quantified by the ratio of the ionospheric electric field to the corotation electric field, α, the total ionospheric electric current, I_{iono}, the Joule heating, and the perturbation magnetic field due to ionospheric currents relative to the background field, $|\Delta B / B_J|$, for which typical values may be found in Table 1. As a result of these interactions large electric currents flow through their ionospheres ($\sim$10, 1.4, 0.15 MA for Io, Europa, and Callisto, respectively) accompanied by respective large Joule heating rates ($\sim$40, 3, $\leq 0.1 10^{10}$ W) that are the dominant heating mechanism of their atmospheres, leading to estimates of high temperatures $\sim$1000–2000 K for altitudes 2 scale heights above their surfaces (cf. Table 1).

The consequences of Callisto's large distance from Jupiter, the large electron and neutral densities and only an induced magnetic field, are a very highly conducting ionosphere with

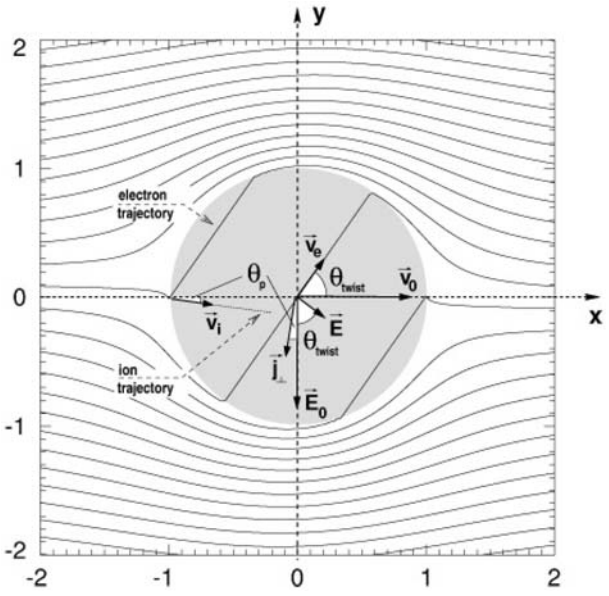

Fig. 10 Isocontours of the electric potential for an illustrative analytic solution with constant conductances $\Sigma_A = 5$, $\Sigma_H = 50$, $\Sigma_P = 25$ S, where the ionospheric field $\vec{E_i} = \vec{E}$, the velocities of the corotation plasma, $\vec{v_0}$, electrons, ions, $\vec{v_i}$, and electrons, $\vec{v_e}$ (from Saur et al. 1999)

conductances on the order of 10^4 mho, that greatly shield the atmosphere from penetration of magnetospheric plasma. One measure of this shielding is the ratio of the ionospheric electric field to the corotation electric field ($\alpha = E_i/E_0$), which is only 0.001 for Callisto in comparison to 0.1 and 0.2 for Io and Europa, respectively.

In order to gain physical insight into magnetospheric interaction with the Galilean satellites, which do not have an intrinsic magnetic field, the analytic Alfven wind model of Saur et al. (1999) is adopted. With the standard magnetospheric Cartesian coordinate system (x in the direction of corotation flow, y directed towards Jupiter and z upward with the magnetic field $\vec{B}$ in the minus z direction), Saur et al. obtained for the ionospheric electric field (cf. Fig. 10)

$$\vec{E}_i = -E_0 \frac{2\Sigma_A}{\Sigma_H^2 + (\Sigma_P + 2\Sigma_A)^2} \begin{pmatrix} -\Sigma_H \\ \Sigma_P + 2\Sigma_A \\ 0 \end{pmatrix}. \tag{1}$$

With the ionospheric conductances much larger than the Alfven conductance, the magnitude of the ionospheric electric field is considerably reduced from the external corotation electric field, $\vec{E_0}$. This is the $\alpha = E_i/E_0$ quantity in Table 1. Note that Hall conductances cause the ionospheric electric field to have a positive component in the x direction and the ionospheric electric field, $\vec{E}_i$, to be rotated counterclockwise from the direction of the corotation electric field, $\vec{E_0}$, by an angle

$$\tan\theta_{twist} = -\frac{\Sigma_H}{\Sigma_P + 2\Sigma_A} \tag{2}$$

(cf. Fig. 10). The perpendicular electric current through one hemisphere of Io is

$$\vec{J}_\perp = -E_0 \frac{2\Sigma_A}{\Sigma_H^2 + (\Sigma_P + 2\Sigma_A)^2} \begin{pmatrix} 2\Sigma_H\Sigma_A \\ \Sigma_H^2 + \Sigma_P(\Sigma_P + 2\Sigma_A) \\ 0 \end{pmatrix}. \tag{3}$$

The perpendicular electric current is rotated clockwise from the direction of the corotation electric field, $\overrightarrow{E_0}$, because of Hall conductance, by an angle

$$\tan\theta_{\rm p} = \frac{2\Sigma_{\rm H}\Sigma_{\rm A}}{\Sigma_{\rm H}^2 + \Sigma_{\rm P}(\Sigma_{\rm P} + 2\Sigma_{\rm A})} \tag{4}$$

(cf. Fig. 10) and generates a small Hall current oppositely directed from the corotation flow. This is also the angle that the incident magnetospheric ions are deflected when entering the highly anisotropic conducting ionosphere. The angle, $\theta_{\rm twist}$, is much larger than the angle, $\theta_{\rm P}$, because $\Sigma_{\rm P,H} \gg \Sigma_{\rm A}$. As a consequence of the current flowing through the highly conducting ionosphere, the Joule heating rate due to dissipation is given by

$$P = 2\pi R_{\rm S}^2 E_0^2 \Sigma_{\rm P} \frac{(2\Sigma_{\rm A})^2}{\Sigma_{\rm H}^2 + \Sigma_{\rm P}(\Sigma_{\rm P} + 2\Sigma_{\rm A})}. \tag{5}$$

The magnetospheric plasma interaction with these atmospheres has been remotely sensed by HST/STIS observations. The regions of brightest UV line emissions from O_I (and S_I on Io) correspond to the regions of maximum deposition of magnetospheric electron power. On Io, some of this UV auroral emission is produced in equatorial spots organized by Jupiter's magnetospheric field and brightest where the field is closest to the surface, but above the limb. Theoretical models can explain why UV emission is preferentially brighter at the equator than the poles (Saur et al. 2000). On Europa with a thinner atmosphere, the UV emission is primarily limb glow with possibly one bright region on the disk. The latter is not understood. On Ganymede UV emission is mostly confined to the auroral oval regions, whereas on Callisto no UV emission has been detected other than resonance scattering of solar Lyman-α by a hydrogen atom corona. For Callisto the absence of UV emission is due in part to the very low magnetospheric electron densities and to strong shielding by the highly conducting ionosphere.

3.2 Titan

As the largest moon of Saturn, Titan has an extensive atmosphere/ionosphere system (Hartle et al. 1982; Nagy and Cravens 1998; Wahlund et al. 2005; Waite et al. 2005; Cravens et al. 2006) with no appreciable intrinsic magnetic field (Ness et al. 1982; Backes et al. 2005). Titan's orbit is at 20 $R_{\rm S}$ ($R_{\rm S}$ is the radius of Saturn) from Saturn and is located inside Saturn's magnetosphere for nominal solar wind conditions. The early knowledge of Titan and its plasma interaction are based on the observations by Voyager 1 spacecraft when it encountered Titan on November 12, 1980 (Ness et al. 1982; Neubauer et al. 1984). The ongoing Cassini mission will have made more than 40 Titan flybys, by the end of its nominal mission. These flybys provide a great opportunity to study in detail Titan's interaction with Saturn's magnetospheric plasma under a wide variety of conditions.

The magnetospheric conditions near Titan play an important role in the evolution of Titan's atmosphere and ionosphere. The corotational plasma proves to be both a source and a loss of ions for Titan. The incident plasma can add a significant amount of H^+ and O^+ into Titan's atmosphere. These ions will in turn deposit their energy in the atmosphere, influencing chemical reactions, ionizing neutral species and heating the atmosphere. In addition the electric and magnetic fields present in the Saturn's outer magnetosphere can pick up ionized species from Titan's ionosphere and thus remove them. In the next section the properties of the plasma near Titan's orbit are outlined. General interaction features are discussed next. The current estimates of the amount of H^+ and O^+ that is deposited into Titan's atmosphere

and estimates of the loss rates for various ionospheric species by the pick up process are also presented.

3.2.1 Plasma Properties Near Titan's Orbit

The plasma conditions in Saturn's outer magnetosphere along Titan's orbit are highly variable. The morphology of the magnetosphere is sensitive to the incident solar wind. Observations of Saturn's magnetospheric magnetic field using the Cassini magnetometer suggest that the magnetic equator is distorted northward (for northern hemisphere winter) not only in the magnetotail, but also on the dayside and flanks (Arridge et al. 2008). Thus, Saturn's magnetic equator and equatorial current sheet form a "bowl-shape" geometry. A magnetodisc is prevented from forming near the sub solar region by the solar wind, but forms tailward of 0900 SLT (cf. Arridge et al. 2006 and references there in). The sensitivity of the magnetosphere to the solar wind means that there is a possibility for Titan to find itself outside of Saturn's magnetosphere in the magnetosheath or even possibly the solar wind. A statistical study by Lundberg et al. (2005) found that for Titan located near the sub solar point, 56.7% of its time would be in the magnetosphere, 42.1% in the magnetosheath and 1.3% in the solar wind. It is not known yet how much of Titan's orbit is spent within Saturn's magnetodisc. The plasma conditions in all of these regions are still being investigated by Cassini. The discussion here is confined to plasma conditions during the initial Cassini flybys of Titan.

The Cassini Plasma Spectrometer (CAPS) observations of the Ta and Tb encounters indicated a flow speed of 120–160 km/s for the incident plasma with respect to Titan (Szego et al. 2005). They also found that the plasma is composed of H^+ and an additional heavy species of mass 14–16 amu. CAPS found the plasma conditions during the TA and T5 encounters to be quite variable. The plasma consists of a mixture of hot, low-density flux tubes and cold, high-density ones. These structures had size scales on order of one Saturn radius (60330 km or about 23 R_T). The electron number density across these flux tubes varied by an order of magnitude centered around 10^{-1} cm^{-3}. The mean temperature of the heavy ion component was found by Cassini to be about 1 keV, compared with 2.9 keV temperature derived by Voyager. Further analysis by Hartle et al. (2006a) found that an additional light H_2^+ species was present. They found that the ambient plasma was hot, with energies of ∼0.16–6.3 keV for H^+, ∼0.1–4 keV for H_2^+ and ∼1–4 keV for O^+. The distribution function of the ambient ion species is often considered to be a Maxwellian. However, analysis by Szego et al. (2005) found that the velocity distribution of the ambient O^+ is a shell. It was shown by Ledvina et al. (2005) that the ambient heavy ion component observed by Voyager could be described in terms of either a Maxwellian or a shell distribution.

In addition to the ion observations made by the CAPS instrument the magnetospheric imaging instrument (MIMI) has observed very energetic (up to a few MeV) H^+ near Titan's orbit. The MIMI instrument has found a difference in their observed ion spectra depending on whether or not Titan is in Saturn's magnetodisc. The ion spectra above ∼600 keV is fairly constant regardless of Titan's location. Below this energy the flux of H^+ is larger when Titan is in the magnetodisc (see Cravens et al. 2008 for further discussion). They also find evidence for very energetic O^+ ions near Titan.

3.2.2 General Interaction Features

Titan's interaction with the Saturnian magnetospheric plasma flow is similar in many ways to the solar wind interaction with Venus/Mars, but normally with subsonic rather than supersonic flow conditions. The subsonic nature means that a bow shock is not expected to form

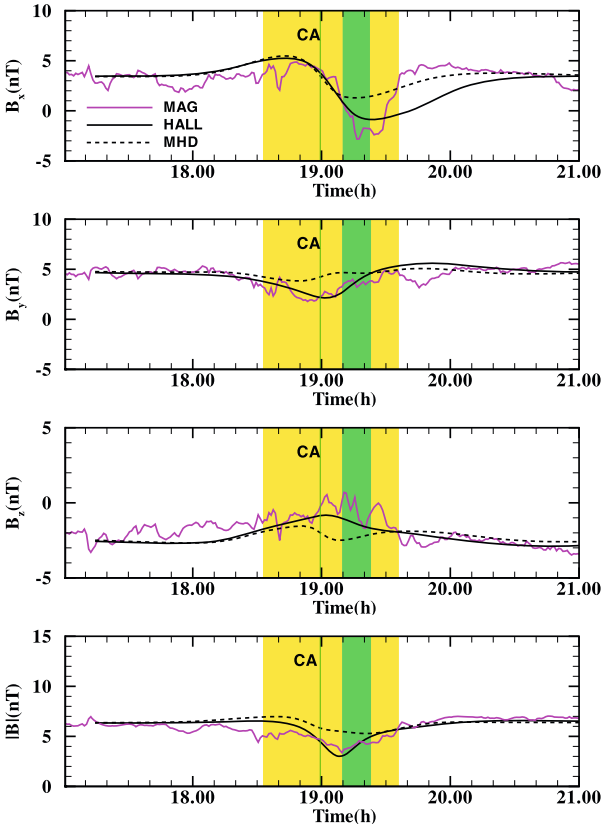

Fig. 11 Model and data comparison of magnetic field along T9 flyby. The green lines indicate the closest approach time. (From Ma et al. 2007a)

in front of Titan. A pair of Alfven wings forms along the magnetic field lines due to perturbations of field-aligned currents (Ness et al. 1982; Luhmann et al. 2004). On the upstream side, Saturn's magnetospheric plasma flow starts to slow down from about 8 R_T (Titan radius) due to mass loading with Titan's extended atmosphere (Hartle et al. 2006a, 2006b), while significant pile-up and strong draping of the magnetic field lines begins around 2 to 3 R_T in front of the satellite. In the tail region, an induced bipolar magnetic tail was observed by Voyager spacecraft and three thin current regions were crossed (Ness et al. 1982). A clear tail structure was seen by the Cassini TA, TB and T3 observations (Backes et al. 2005; Neubauer et al. 2006), as the magnetic field reversed direction suddenly when Cassini passed from one magnetic tail lobe to the other. The wake region is highly dynamic, and both the location and width of the current sheet are closely related to the upstream plasma pressure and magnetic field directions.

The Cassini spacecraft passed through the distant downstream region of Titan at 18:59:30 UT on Dec. 26, 2005, which is referred to as the T9 flyby. This flyby provided important information of the highly dynamic wake region and has been discussed in detail by a series papers in a special issue of *Geophysical Research Letters* (Bertucci et al. 2007; Wei et al. 2007; Coates et al. 2007; Kallio et al. 2007; Simon et al. 2007). Figure 11 shows the comparison between the calculated and observed magnetic field values along the T9 trajectory for plus and minus 2 hours of closest approach (CA) from Ma et al. (2007a). The overall trends of magnetic field vectors, especially the sharp decrease of B_X, are reasonably well repro-

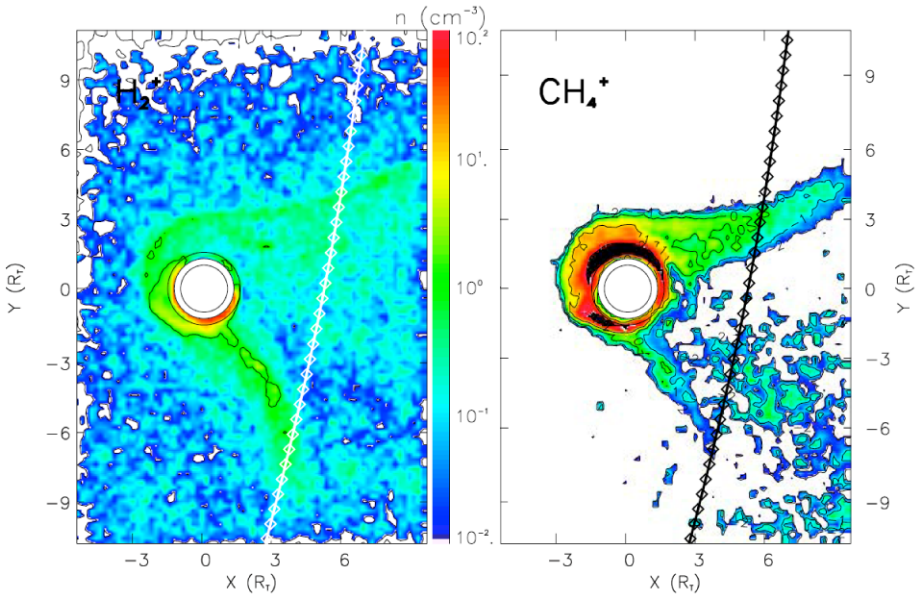

Fig. 12 Density maps of (*left*) H_2^+ and (*right*) CH_4^+ in the XY plane of Titan. The trajectory of Cassini is indicated in the simulation coordinate system. (From Modolo et al. 2007a)

duced by the Hall MHD model, indicating the importance of kinetic effects in the interaction process. They also discussed in detail why the Hall MHD model results fit the observations fairly well even when the ion gyroradii of upstream plasma ions are larger than Titan's size. A difference in the plasma composition, between the inbound and outbound segments of the flybys was observed by the CAPS experiment (Szego et al. 2007). Heavy ions of mass 14–18 AMU and mass 30 AMU were only observed on the Saturn-facing edge (positive Y direction) of the wake while the light ions with an ion mass of 2 AMU are present on the anti-Saturn edge (negative Y direction). As shown in Fig. 12, such features were successfully reproduced by Modolo et al. (2007a).

Although there is significant magnetic enhancement in the upstream region close to Titan, no statistical study of the location of the magnetic pile-up boundary has been performed. Clear ionopause signatures have been observed at Titan only during one Cassini pass to date: T34 flyby (Ma et al. 2007b). During this pass, Titan was located near 18 SLT, so that the upstream region was corresponding to the dayside ionosphere. The spacecraft passed through the upstream equatorial plane. As can be seen from Fig. 13, the magnetic field strength drops sharply near the closest approach, corresponding to what could be considered an ionopause around 1500 km. Since the peak ionospheric thermal pressure in the upstream region varies significantly when Titan moves along its orbit, whether the ionopause exists or not during other Titan orbital location is still an open question.

3.2.3 Ambient Ion Fluxes into Titan's Atmosphere

The gyroradii of the ambient ions can be significant when compared to the size of Titan. For instance the gyroradius of a 5 keV H^+ and O^+ ion is 0.79 R_T and 3.2 R_T respectively. The trajectories of ambient ions near Titan have been simulated by Ledvina et al. (2000,

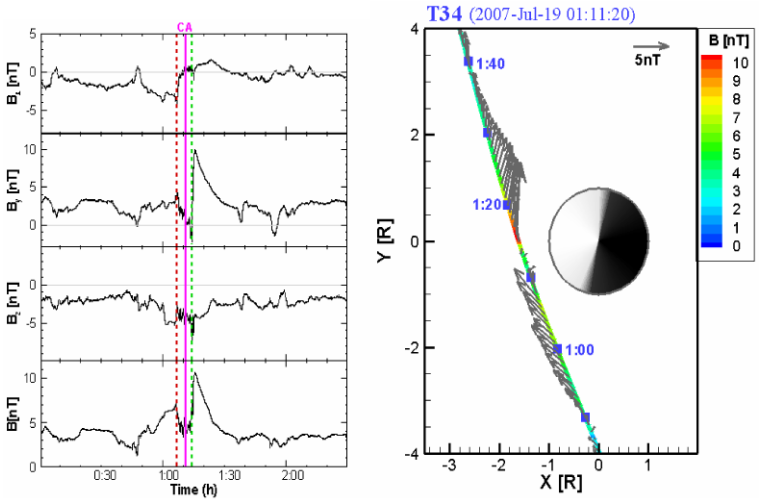

Fig. 13 Cassini Magnetometer observation during T34 flyby. The *dashed lines* indicate the ionopause locations (Ma et al. 2007b)

2005). They combined the electric and magnetic fields from a MHD simulation of Titan's plasma interaction during the Voyager encounter, with a Monte Carlo/test particle approach. Their approach though not self-consistent was able to predict, describe and explain much of the collective ion behavior near Titan. They argue that the larger the ion gyroradius the less sensitive the ambient ion is to Titan's induced magnetic field and the more likely it is to enter Titan's atmosphere. Their simulations predicted that most of the ambient H^+ ions (energies <3 keV) are shielded from Titan's atmosphere by its induced magnetic field. In contrast the heavier ambient ion species were much less sensitive to the induced magnetosphere and easily entered Titan's atmosphere. They further calculated that for conditions present during the Voyager 1 encounter 3.9×10^{22} H^+ ions/s would enter Titan's atmosphere. The ion flux into Titan's atmosphere was found to be dependent on the distribution function for the heavy ambient ion species. If the heavy ambient ion species had a Maxwellian distribution then 1.7×10^{24} ions/s entered Titan's atmosphere. This flux dropped to 2.9×10^{23} ions/s if the distribution function was a shell.

Recent self-consistent hybrid simulations by Sillanpää et al. (2007) calculate a flux of 1.3×10^{24} ions/s of O^+ entering Titan's atmosphere using a ambient Maxwellian distribution. They found an H^+ flux of $1.3–1.4 \times 10^{23}$ ions/s. This is more than twice that of the Ledvina et al. (2005) result. Sillanpää et al. (2007) attribute this to the symmetric field results in the MHD simulation used by Ledvina et al. (2005). Another possibility is that Ledvina et al. (2005) did not allow for the possibility of H^+ ions moving along the draped field towards Titan. This effect was included in the Sillanpaa et al., simulation. What the difference in these results illustrates is that the H^+ flux into Titan's atmosphere is sensitive to the configuration of Titan's induced magnetosphere.

Hartle et al. (2006a) reported that both the Voyager PLS instrument and the Cassini CAPS instrument observed an O^+ clearing region around Titan. From these observations they estimated that Titan absorbs $\sim 5.6 \times 10^{23}$ ions/s of ambient O^+. They are quick to point out that the interaction region is complex requiring a full 3D kinetic treatment for a more accurate rate. Still their estimate is within a factor of 3 of the estimates given above.

There has been much interest recently in the very high energy H^+ ions observed by MIMI and their atmospheric consequences. The MIMI team (D. Mitchell, private communication) has observed ions (mostly H^+) precipitating into Titan's atmosphere below an altitude of 1000 km. They estimate that these precipitating ions (energies above 10 keV) deliver from 5×10^{-5} to 5×10^{-3} ergs/cm^2/s to Titan's atmosphere below 1000 km. Energetic O^+ is often present, but they have not surveyed its contribution to the energy deposition yet. Recently Cravens et al. (2008) have examined the atmospheric consequences of these energetic ions. They found that these precipitating ions can lead to significant ionization around 600–800 km, which is well below the altitude of the peak ion production from photoionizataion. This ionization process may explain recent ionospheric layers observed by the radio occultation observations at Titan (Kliore et al. 2007).

3.2.4 Pickup Ion Fluxes into Titan's Atmosphere

Another source of ion precipitation into Titan's atmosphere comes from Titan itself. Neutrals in Titan's upper atmosphere and exosphere can become ionized. These ions can be picked up by the surrounding plasma flow and be accelerated back into Titan's atmosphere. This can in turn heat the atmosphere. The motional electric field that picks up the ions is directional so these ions will tend to be accelerated away from Titan in the anti-Saturn facing hemisphere and into Titan on the Saturn facing hemisphere. This will result in asymmetric heating of the atmosphere.

The study of Ledvina et al. (2005) also examined the re-entering pickup ions. They found that 1.4×10^{22}, 5.6×10^{23} and 8.7×10^{23} ion/s for 1, 14 and 28 amu ions re-entered Titan's atmosphere. Most of these ions tended to impact the Saturn facing hemisphere of Titan. However, they found that Titan's induced magnetosphere also allowed a fair amount of ion energy to be deposited in the anti-Saturn hemisphere. In this study a symmetric ionosphere was produced which is a significant model limitation since it is known that photoionization is directional.

Tseng et al. (2008) improved upon the study of Ledvina et al., by removing the symmetry assumptions. They used the field output from a MHD simulation of Titan's plasma interaction at different regions in Saturn's magnetosphere. Thus these fields were not symmetric about Titan but included the effects of a solar zenith angle production source. They also ran a symmetric case for comparisons with Ledvina et al. (2005). They found that their ion fluxes ranged from 2.22–2.31 $\times 10^{22}$ ions/s for H_2^+, 3.33–4.56 $\times 10^{23}$ ions/s for CH_4^+ and 5.70–8.02 $\times 10^{23}$ ions/s for N_2^+. These values are in good agreement with the estimates of Ledvina et al. (2005). The variations are due to the change in the solar zenith angle. Both Tseng et al. (2008) and Ledvina et al. (2005) are also in agreement with the estimated pickup ion energy deposited into Titan's atmosphere.

Michael and Johnson (2005) used a direct simulation Monte Carlo (DSMC) method to study the energy deposition and heating of Titan's upper atmosphere. They found that pickup ions can deposit more energy near the exobase than solar radiation. However sputtering and collisional transport to the lower atmosphere causes this energy to be lost resulting in a temperature increase near the exobase of just a few degrees.

3.2.5 Ion Loss from Titan

Neutral species becoming ionized and getting picked up by the motional electric field is thought to be one of the chief loss mechanisms at Titan. This process was examined by Ledvina et al. (2005). They found that Titan's induced magnetosphere could act to prevent

ions from being picked up by the external flow or even scatter some of the ions back into Titan. They calculated that the pick up process would result in a loss of 6.6×10^{23}, 7.4×10^{23} and 6.3×10^{23} ions/s for 1, 14 and 28 amu pick up ion species. Most of these ions would have energies of less than 3 keV near Titan. Their velocity space distributions would be non-gyrotropic rings.

MHD simulations computed with upstream plasma parameters similar to those encountered for Ta and Tb encounters, gave an estimate of the total ion escape fluxes of 5.1×10^{24} ions/s and 2.6×10^{24} ions/s respectively (Ma et al. 2006). Hybrid simulations performed by Sillanpää et al. (2006) indicate a net outflow of methane ions, of the order of 1.1×10^{25} ions/s, with different Titan's orbital positions. Hybrid simulation by Modolo et al. (2007a) performed with the T9 conditions, suggests a total escape flux of 5.6×10^{25} ions/s (with a contribution of 1.3, 2.4 and 1.9×10^{25} ions/s for N_2^+, CH_4^+ and H_2^+ respectively).

Observations of pickup ions by the CAPS instrument are reported in Hartle et al. (2006a). They find that the principal pickup ion species are H^+, H_2^+, N^+, CH_4^+, and N_2^+. Hartle et al. (2006a) state that the pickup ion distribution function should be a ring. However, close to Titan the distribution can be interpreted in terms of narrow energy ion beams. This is because the ion gyroradii are much larger than the scale height of the source neutral profile. To the best of our knowledge CAPS has not yet published estimates of the pickup ion loss rates. However, Eviatar et al. (1982) estimated a net loss of 3×10^{24} ions/s based on the Voyager encounter. The total ion outflow is estimated at $2–7 \times 10^{25}$ ions/s based on Langmuir Probe observations of the T9 flyby, if one assumes a cylindrical geometry for the plasma wake (Modolo et al. 2007b). Further observations and simulations are needed to better understand the extent of atmospheric loss by the pickup process.

4 Comets

Comets are small solar system bodies surrounded by extensive dusty atmospheres that evolve along their orbit. The plasma environment around comets is affected by the cometary dust and gas coma, as well as the persisting solar wind. Most of our current knowledge of comets and their plasma environment are based on optical observations using telescopes, and direct observations from a few flybys to comets 21P/Giacobini-Zinner, 1P/Halley, 26P/Grigg-Skjellerup and 19P/Borrelly. Nevertheless, the plasma environment around comets provides us a unique laboratory filled with current systems, waves and dynamic boundaries. Most of the experimental evidence on ionospheres of comets comes from the Giotto mission to comet 1P/Halley in 1986 and to comet 26P/Grigg-Skjellerup in 1992. The most surprising cometary ion data were probably the data gathered with the solar wind experiment and the magnetometer on the solar mission Ulysses 3.4 AU away from comet C/1996 B2 (Hyakutake) and 1.6 AU away from C/2006 P1 (McNaught).

4.1 Overview of the Comet Interaction with the Solar Wind Plasma

Neutral atoms and molecules of cometary origin that are released by the sublimation of dusty/icy mix of the upper several centimeter layers at the surface of the cometary nucleus move along ballistic trajectories and become ionized with a characteristic ionization lifetime of 10^6–10^7 s. Freshly born ions are accelerated by the motional electric field of the high-speed solar wind flow. The ion trajectory is cycloidal, resulting from the superposition of gyration and $\mathbf{E} \times \mathbf{B}$ drift. The corresponding velocity-space distribution is a ring-beam distribution, which has large velocity space gradients and is unstable to the generation of low frequency transverse waves. The combination of ambient and self-generated

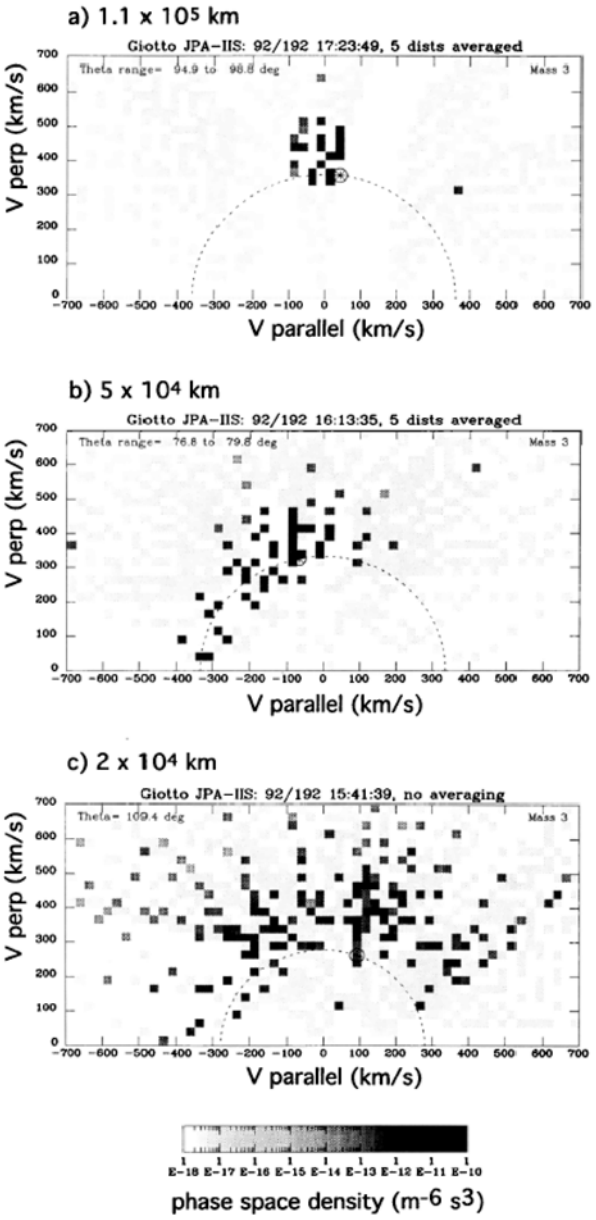

Fig. 14 Examples of the water group ion distributions observed by the Giotto IIS at distances of (**a**) 1.1×10^4 km, (**b**) 5×10^4 km, and (**c**) 2×10^4 km on the G-S outbound pass. Measured zeros are represented by a *light shade of grey*. Areas left white are outside the instrument field of view. Reprinted from Huddleston et al. (1993)

magnetic field turbulence pitch-angle scatters the newborn ions from the pickup ring. As a result of this process the pitch angles of the pickup-ring particles are scattered on the spherical velocity space shell around the local solar wind velocity (e.g. Galeev et al. 1991; Neugebauer et al. 1991; Motschmann and Glassmeier 1993; Coates et al. 1993). Water group ion distribution functions were measured by the Giotto spacecraft during the flyby of comet Grigg-Skjellerup at a range of distances from the nucleus showing the evolution of the pickup ring distribution. See Fig. 14 from Huddleston et al. (1993).

Conservation of momentum and energy causes the solar wind to be decelerated as newly born charged particles are picked up by the magnetized plasma flow. Continuous deceleration of the solar wind flow by mass loading occurs until a weak shock forms and the flow becomes subsonic. The cometosheath is located between the cometary shock and the magnetic field free region in the innermost coma. The plasma population in the cometosheath is a changing mixture of ambient solar wind and particles picked up upstream and downstream of the shock. Near the nucleus ion–neutral chemistry and recombination starts to become more and more important. In the inner coma, an "ionopause" separates the solar wind controlled magnetized plasma from the magnetic field-free cometary ionosphere, the diamagnetic cavity. Deep inside the diamagnetic cavity the cometary plasma and the neutral gas are very strongly coupled by ion–neutral collisions (Cravens et al. 1991a, 1991b), and they move radially outward with the same expansion velocity.

Weaker Jupiter family comets, like the Rosetta mission target comet 67P/Churyumov-Gerasimenko, will only have a small diamagnetic cavity and only for heliocentric distances less than ∼2 AU (Hansen et al. 2007). For Halley-class comets and brighter at moderate to small heliocentric distances an extensive set of ion-molecule reactions are responsible for determining the ion composition in comets beginning with an initial set of primary photoionization products (Häberli et al. 1997; Rodgers et al. 2004). The main photoionization product in the cometary coma is H_2O^+. These water ions transfer a proton to other neutral molecules, which have a higher proton affinity than the OH radical. The prime example is $H_2O^+ + H_2O \rightarrow H_3O^+ + OH$, but there are other similar reactions that result in the creation of species like HCO^+ that was detected in comet 1995 O1 Hale-Bopp (Lovell et al. 1999) owing to the large diamagnetic cavity of 30,000 km (Gombosi et al. 1997) that results from its huge gas production rate. The proton affinity of the parent molecules determines the reaction rate; therefore protonated ions of molecules with high proton affinity are more abundant (relative to other ions) than ions of their parent molecules (relative to other neutrals) (Häberli et al. 1997). Therefore, the most important reaction in the innermost coma is proton transfer, e.g.

$$H_3O^+ + M \rightarrow H_2O + MH^+ \tag{6}$$

which leads to typical ion mass spectra where the uneven mass numbers contain the highest peaks, due to the fact that C and O containing molecules can be found at even mass numbers, e.g. mass 31 amu/e (CH_2OH^+, protonated formaldehyde) or mass 33 amu/e ($CH_3OH_2^+$, protonated methanol) (Fig. 15).

Further out or in weaker comets, ion–molecule reactions become less important relative to photo-reactions and the most important ion is then the water ion H_2O^+. Even further away from the nucleus molecular ions are slowly replaced by atomic ions. Inside the so-called magnetic cavity ions and neutrals are in a local chemical equilibrium. The ion population therefore strongly follows the neutral composition. Outside of the cavity this local chemical equilibrium is no longer maintained for all species. The neutral and the ion composition decouple. A good example for this behavior is the sulfur ion. Whereas the densities of most of the other ion species decrease in a monotonous fashion over the magnetic cavity boundary following the decrease in the neutral density, sulfur ions are piled up right at the boundary (see Fig. 16). This is due to the fact that the sulfur ion has a very long lifetime. Sulfur ions produced far away upstream from the magnetic cavity are flushed back by the solar wind towards the comet nucleus and pile up at the magnetic cavity boundary, the contact surface. They are no longer in local chemical equilibrium with the neutral parent species.

In situ measurements of the immediate cometary plasma environs are limited to the ICE flyby of comet 21P/Giacobini-Zinner, the Giotto flybys of comet 1P/Halley and 26P/Grigg-

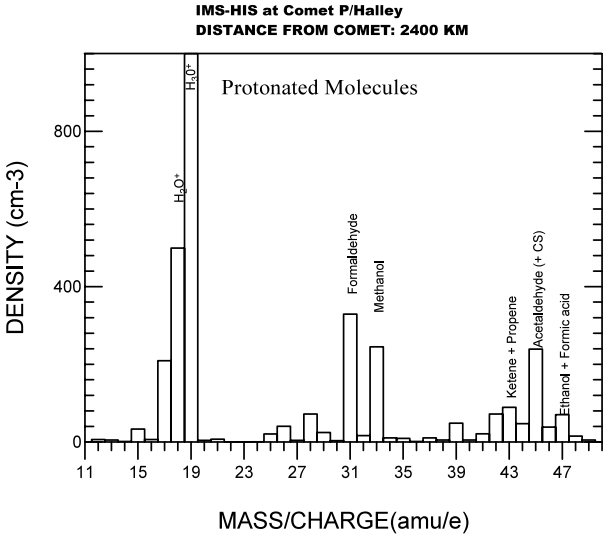

Fig. 15 Ion mass spectrum from the Giotto IMS-instrument

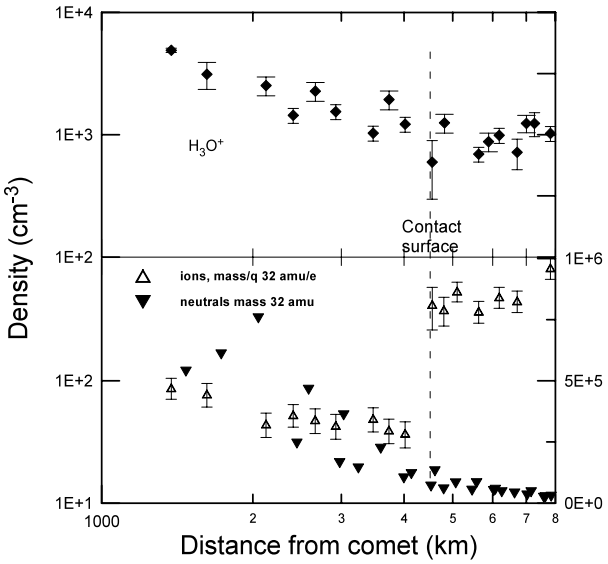

Fig. 16 Data from Giotto during the 1P/Halley flyby: Ion data from the IMS-instrument and neutral data from the NMS-instrument. *Upper panel*: mass/charge 19 amu/ which is due to the hydronium ion; lower panel: mass/charge 32 amu/charge (*left axis*) and neutral mass 32 amu (*right axis*) respectively. The discontinuity of the sulfur ions at the contact surface is due to the long lifetime of these ions

Skjellerup and the flyby of comet 19P/Borrelly by the Deep Space 1 spacecraft. The general features seen in these measurements have been shown to be reasonably reproduced by magnetohydrodynamic (MHD) models of the interaction of the solar wind with the cometary atmosphere (Wegmann 2000; Gombosi et al. 1997; Benna and Mahaffy 2007; Jia et al. 2007). Figure 17 shows steady-state model results for a moderately bright comet at 1 AU from the Sun and showing the classical field-line draping as well as all the normal predicted features, including the upstream bow shock and the inner contact surface and diamagnetic cavity. This result by Jia et al. (2007) is from the latest generation of MHD models implemented on massively parallel computers with a highly refinable computational mesh that can simultaneously resolve small scale phenomena (e.g. shocks and small distances within

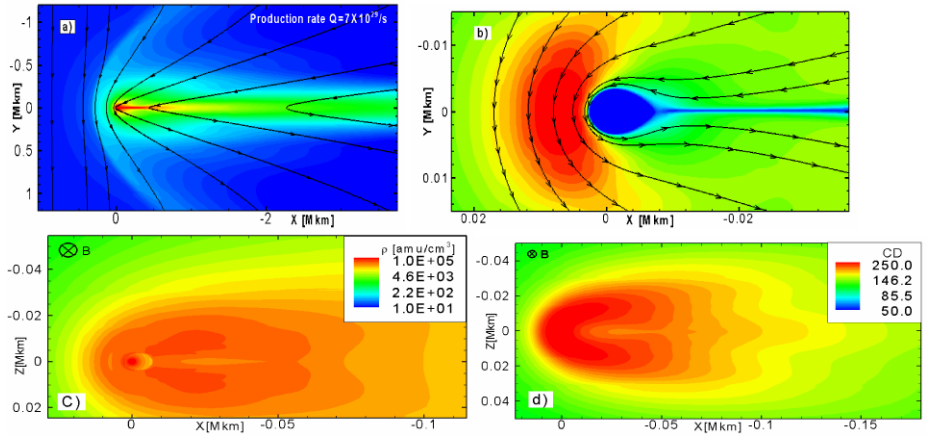

Fig. 17 A comet interacting with a steady-state solar wind. The results of Jia et al. (2007) for the various plasma structures for a moderately bright comet near 1 AU are shown. Magnetic field lines are the *black lines* projected onto the plane containing the interplanetary magnetic field (IMF). **a**) Density contour showing the position of a mass-loaded bow shock. **b**) Magnetic field strength contours in the ecliptic plane showing the structure of the contact surface. **c**) Total ion density contours in the plane perpendicular to the IMF showing the structure of the contact surface and thick tail. **d**) Total ion column density contours in the plane perpendicular to the IMF showing the broad tail. (From Jia et al. 2007)

the contact surface) as well as the global interaction. The more distant plasma tails of comets 1996 B2 Hyakutake (Gloeckler et al. 2000; Jones et al. 2000) and 2006 P McNaught (Neugebauer et al. 2007) have been serendipitously intercepted by the Ulysses spacecraft in 1996 and 2007, respectively. These *in situ* measurements show singly-ionized cometary pickup ions as well as multiply charged C^{++}, O^{++} and O^{3+} which could be cascaded intermediate charge-state heavy solar wind ions, which produce cometary X-rays (Lisse et al. 1996; Cravens 1997b), as well as the surprisingly continuing disturbed solar wind flow even more than 2 AU down stream of the comets.

When comet Hyakutake (C/1996 B2) was observed with the Röntgen Satellite (ROSAT) surprisingly strong X-ray emission was observed (Lisse et al. 1996). The emission morphology was symmetric with respect to a vector from the comet's nucleus toward the sun, but not symmetric around the direction of motion of the comet with respect to interplanetary dust. Observations of other comets in this wavelength range indicate that X-rays are produced by almost all comets. Theoretical and observational work has demonstrated that charge-exchange collisions of highly charged solar wind ions with cometary neutral species can explain this emission. The solar wind contains a large number of minor/heavy ion species with a range of charge states, such as O^{6+}, C^{5+}, N^{5+}, and Si^{10+}. These ions will readily charge transfer with cometary neutrals, producing ions that can be highly excited and consequently emit photons in the extreme ultraviolet and X-ray part of the spectrum. X-ray observations of comets and other solar system objects should be able to provide information on the structure and dynamics of the solar wind flow around these objects (Cravens 1997b).

The ion gyroradius for low activity comet is large compared with the length scale of the comet as an obstacle in the solar wind. In this situation the MHD approximation breaks down and the comet solar wind interaction needs to be considered as a kinetic problem rather than a fluid problem. In such cases hybrid kinetic simulations of comets have been made (Lipatov et al. 1997, 2002; Bagdonat and Motschmann 2002a, 2002b). A careful study of MHD and kinetic simulations for the Rosetta mission target comet 67P/Churyumov-Gerasimenko over

the wide range of production rates during its orbit has been done by Hansen et al. (2007). When the comet is nearer perihelion, the hybrid kinetic and MHD simulations give very similar results and a more or less conventional comet/solar wind interaction is present. When the comet is at larger heliocentric distances and has a correspondingly lower production rate, the interaction totally changes character. By 3 AU from the Sun the antisunward directed ion tail totally disappears, and cometary ions simply travel on individual ion-cycloid pickup rings about the direction of the interplanetary magnetic field.

The general aspects of the cometary phenomenon, the production of its neutral dusty-gas atmosphere and its importance to broader planetary studies, specifically the chemistry and physics of the origin and early evolution of the solar system, are discussed in an accompanying papers/chapters by Müller-Wordarg et al. (2008) and Johnson et al. (2008). Ip (2004) presents the most recent up-to-date comprehensive review of the cometary plasma environment. Recent work in modeling the cometary plasma environment has been undertaken to address several important new avenues. Numerical and computational advances have enabled modeling the time dependent phenomena in cometary plasmas such as testing for the causes of the long observed cometary tail disconnection events. Voelzke (2005) presents a review of the past work in this area (Schmidt-Voigt 1989; Wegmann 2000; Yi et al. 1996). Konz et al. (2004) have also explored reconnection events in the context of a 2D resistive MHD calculation. Jia et al. (2007) have tested various types of the tangential solar wind discontinuities that would be expected of a heliospheric current sheet crossing were the trigger for disconnection events as suggested by Brandt and coworkers (Niedner and Brandt 1978; Brandt et al. 1999). They find that the passage of various tangential discontinuities produce cometary tail rays, but only field-flips of greater than 90° when viewed from the appropriate direction with respect to the ambient interplanetary magnetic field direction produce both detectable tail disconnections as well as cometary tail rays. Furthermore they are able to reproduce the recession speeds of the disconnected tail. Figure 18 shows results of Jia et al. (2007) for a time-dependent calculation of a 180° tangential discontinuity passing by a moderately bright comet. In this case the observational geometry with respect to the upstream IMF is not favorable for actually seeing the disconnection, however the appearance of tail rays is quite similar to observations of comet Austin by Bonev and Jockers (1994). The figure shows the event in various stages of the interaction using the disconnection phase nomenclature of Brandt (1982) and Brandt and Chapman (2004).

Benna and Mahaffy (2007) have performed 3D multi-fluid MHD model calculations for the interaction of the solar wind with comet 1P/Halley corresponding to Giotto spacecraft flyby conditions. They include ions, neutrals and electrons as separate interacting fluids. Their comparison with both various Giotto spacecraft data as well as derived quantities compares quite favorably, as had the earlier single-fluid MHD model of Gombosi et al. (1996). In the earlier work the electron temperature was determined separately and imposed on the MHD simulation, whereas in the newer work similar physical assumptions are used to calculate the electron temperature more self-consistently within the MHD calculation itself.

4.2 Tangential Discontinuity and Diamagnetic Cavity; Ionospheric Acceleration and Deceleration

The plasma in the inner coma of an active comet like Halley becomes rather slow (speeds of a few km per second or less) and the cometary plasma density builds up to higher values ($n_e \approx 10^3$–10^4 cm^{-3}). Collisional processes, including chemistry become important in this "cometary ionosphere" (see accompanying paper by Witasse et al. 2008; Cravens 1991a, 1991b). For example, the main ion species for distance less than 2×10^4 km is mass 19

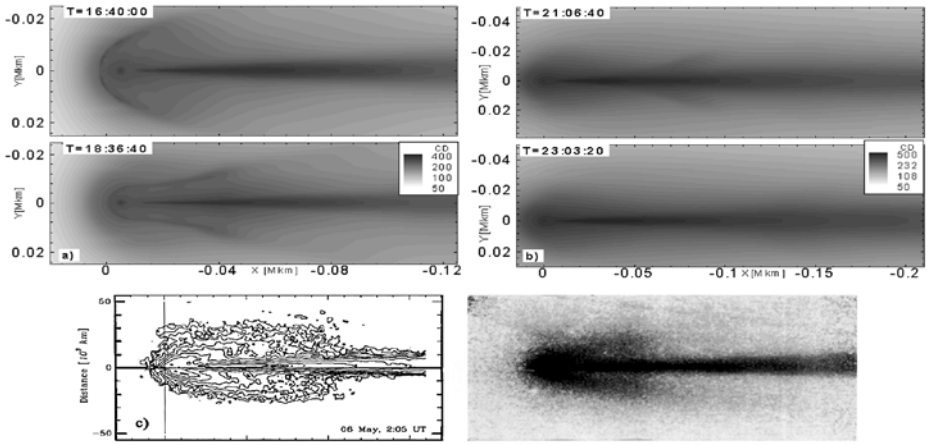

Fig. 18 Comparison of time-dependent MHD model results with observations. Images looking along the direction of the upwind interplanetary magnetic field: Column densities showing tail rays with no observable disconnection in units of 6×10^{10} amu/cm^2. **a**) Phase I. **b**) Phase II–IV, tail rays folded into the tail, but no disconnections can be observed. **c**) Column density of water ions in comet Austin, May 6, 1990, the distances are 10^4 km. Figures **a** and **b** from (Jia et al. 2007), figure **c** from (Bonev and Jockers 1994)

(H_3O^+) rather than H_2O^+ (the main ion produced by photoionization) due to a reaction of H_2O^+ with neutral water (Altwegg et al. 1999). Dissociative recombination is the main loss of plasma in the inner coma, and not transport, with a photochemical density variation that varies inversely with radial distance.

The magnetometer onboard the Giotto spacecraft observed a diamagnetic cavity surrounding the nucleus of Halley at a distance of about 5000 km (Neubauer 1987). The existence of this cavity was successfully explained in papers by Ip and Axford (1987), Cravens (1986, 1989), Puhl-Quinn and Cravens (1995), and Gombosi et al. (1997). Inside the field-free cavity the plasma is coupled with the neutral gas by ion-neutral collisions. Both the ions and the neutrals flow radially away from the nucleus at speeds of about $u_n \approx 1$ km/s. However, in the magnetic barrier outside the diamagnetic cavity boundary the ions are "tied" to the field lines and the neutrals continue to flow outward. In this region an outward ion-neutral friction force of neutrals flowing past stagnated ions is exerted on the plasma. This outward force is balanced by an inward $\mathbf{J} \times \mathbf{B}$ force associated with the magnetic barrier as represented by the following approximate force balance relation:

$$\mathbf{J} \times \mathbf{B} \cong -\nabla(B^2/2\mu_0) = -n_e m_i k_{in} n_n \mathbf{u}_n \tag{7}$$

where n_e is the electron density, m_i is the average ion mass ($\approx$19 amu), n_n is the neutral density, k_{in} is an ion neutral collision coefficient, and u_n is the neutral flow velocity. The $\mathbf{J} \times \mathbf{B}$ force is approximately given by the magnetic pressure gradient force right near the cavity boundary and if the pressure gradient is approximated by the derivative with respect to the radial distance, r, and for a simple $1/r^2$ and $1/r$ (photochemical equilibrium) variations of the neutral and electron densities, respectively, then a simple solution results from integrating this equation is (Cravens 1986):

$$\begin{aligned} B &= B_0\sqrt{[1-(r_{cs}^2/r^2)]} \quad \text{for } r > r_{cs}, \text{ and} \\ B &= 0 \quad \text{for } r < r_{cs} \end{aligned} \tag{8}$$

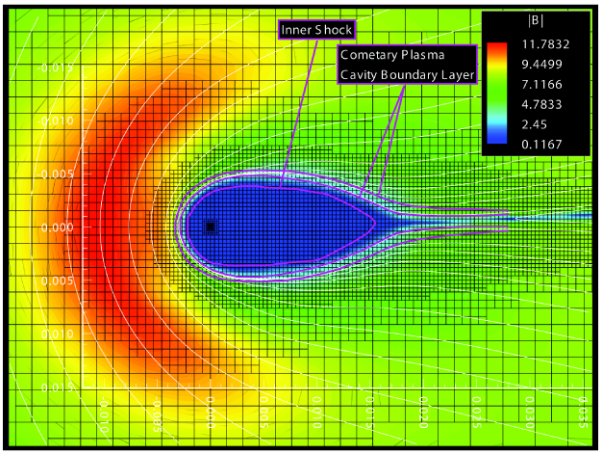

Fig. 19 Magnetic field strength (*color scale* shown in figure) and field lines in the inner coma of comet Halley from a numerical global 3-dimensional MHD model. (From Gombosi et al. 1996)

where B_0 is the field in the magnetic barrier and the radial distance to the diamagnetic cavity boundary for an active comet was found to be given by $r_{cs} = 1.07 \times 10^{-13} Q^{3/4}/B_0$ where Q is the total gas production rate of the comet in units of s^{-1} and B_0 is in units of tesla.

Global MHD models of the cometary plasma environment have reproduced the diamagnetic cavity feature of active comets (e.g., Huebner et al. 1991; Gombosi et al. 1996; Lindgren et al. 1997). Figure 19 shows some magnetic field strengths from a MHD model indicating that the cavity is stretched in the tailward direction, merging with the cometary plasma tail.

5 Ionosphere–Magnetosphere (I-M) coupling

5.1 Terrestrial I-M Interactions

The near-planetary environment, within magnetospheric systems with an ionosphere, can become quite complex. This is because the exchange of mass, momentum and energy between the two is highly nonlinear. It is often extremely difficult to study the magnetosphere-ionosphere coupling because of its complex nature. At many planetary systems, the ionospheric conductivity is uncertain to factors of as much as ten (Eviatar and Richardson 1986; Cheng and Waite 1988; Bunce et al. 2003). Even at Earth, there are many studies that are just attempting to understand the magnitude of the ionospheric conductivity, especially in the dark ionosphere, where the electron density can be difficult to measure. Typically, the conductivity is calculated through the measurement of the electron density and an assumption about the neutral density, or measurement of both, if possible (e.g., Brekke et al. 1974).

One of the best-known processes that give rise to atmospheric plasma flows on Earth is the Dungey (1961) cycle. This process gives rise to a two-cell structure across the auroral/polar regions, in which ionospheric plasma flows in the anti-sunward direction from noon to midnight, and then returns sunward along the dawn and dusk flanks. The process is best understood by considering the reconnection of the Interplanetary Magnetic Field (IMF) lines with the terrestrial field lines at the front of the magnetosphere. The result is that terrestrial field lines that were closed at the front of the magnetosphere are now open and connected to the solar wind. These reconnected field lines are then dragged along by

the on-flowing solar wind, and the ionospheric plasma at their footprints in the atmosphere is dragged along with them (cf. Kelley 1989; Schunk and Nagy 2009). Were this process to continue indefinitely, the entire terrestrial field would be connected to the IMF. But as the now-open field lines are swept back into the magnetotail, they move inwards towards the mid-plane where they can reconnect once more, and drift from the midnight–dawn or midnight-dusk sector back towards noon. For Earth, this whole cycle lasts about 3 hours, or 0.125 of a planetary rotation.

One of the most important considerations, from the magnetospheric stand point, is the closure of the currents generated by this reconnection cycle through the ionosphere. The dense ionospheric plasma, mixed with a neutral gas that is typically many orders of magnitude more dense, allows large conductivities to form, serving the purpose of allowing magnetospheric currents to close. This, in fact, serves an additional role—namely the horizontal current allows a diffusion region to form in the ionosphere, such that the field-lines below the ionosphere (which are frozen to the planet) slip away from field-lines above the ionosphere, which are driven strongly by electric fields from the external medium (i.e., the solar wind in most cases). The ionospheric conductance, therefore, allows there to be convection in the magnetosphere. Simplistically, it regulates the speed of the convection—a large conductance slows the fields down, while a smaller conductance allows very large electric fields and therefore very fast flows (Fedder and Lyon 1987; Ridley et al. 2004).

The coupling between a planetary magnetosphere and its ionosphere is not simply just field-aligned currents. Figure 20 illustrates the complex interaction that occurs between the two regions. This figure illustrates what would pass back and forth between different models of the regions. There are typically three feedbacks between the ionosphere and magnetosphere that are studied: (1) the effect of the ionospheric conductivity on the generation of electric fields within the ionosphere and magnetosphere; (2) the neutral wind dynamo effect on magnetospheric convection; and (3) the effect of ionospheric outflow on the magnetosphere.

As stated above, the ionospheric conductivity has a very large uncertainty in is value. Further, the conductivity actually is a tensor that has three-dimensional structure. Lastly, the conductivity cannot be directly measured, and so it must be inferred by different techniques. This makes setting the ionospheric conductivity in models (and validating them) quite difficult. The structure of the ionospheric conductivity strongly affects where currents will flow and how the ionosphere will interact with the thermosphere. The neutral winds are strongly influenced by ion drag, which is directly related to the conductivity, and the frictional heating in the thermosphere is also controlled by the conductivity. Various studies have examined how the global conductivity can affect the flow patterns in the magnetosphere.

One of the most difficult couplings to understand between the ionosphere and magnetosphere is in the particle precipitation, which strongly controls the conductance in the ionosphere. If one simply considers the electrons, there are many different sources for the precipitation: (1) the central plasmasheet that causes the diffuse aurora; (2) the reconnection site that causes the discrete aurora; (3) the ring current interaction with the plasmasphere which can drive pitch angle scattering into the loss cone and a diffuse aurora to form equatorward of the nominal oval; (4) the radiation belts can cause high energy electrons to precipitate at low latitudes; (5) the cusp allows direct entry of magnetosheath plasma into the ionosphere; and (6) polar rain on open field-lines can be caused by streaming electrons on the interplanetary field-lines. Each of these different source populations has different dynamics that are controlled by different processes, although many of the processes may be interlinked. For example, different models of substorm physics may be dependent upon the underlying conductivity in the ionosphere, caused by the diffuse aurora. If this conductivity is too low, then reconnection in the tail is inhibited and,

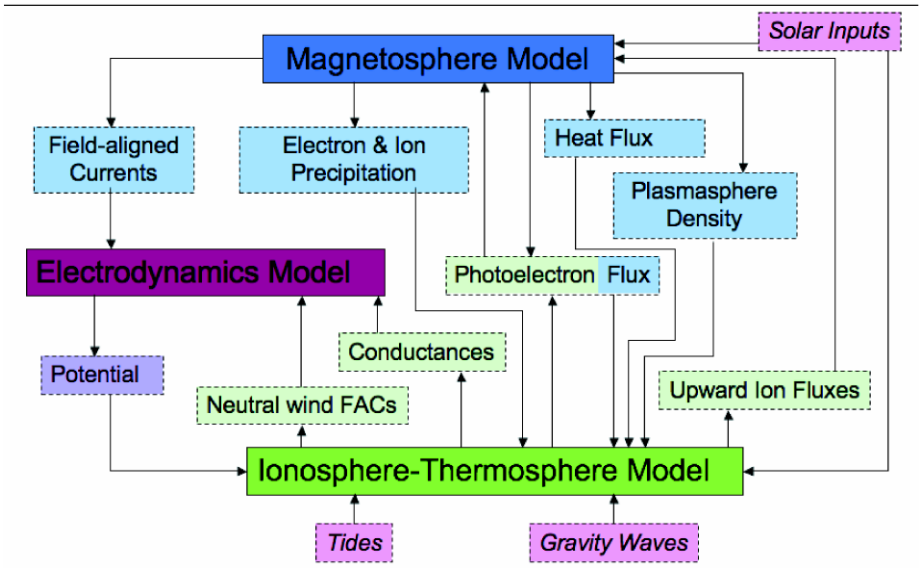

Fig. 20 The flow of information from different models describing the magnetosphere–ionosphere system. The *dark blue*, *purple* and *green boxes* represent models, while the *lighter colors* represent what the model would provide (for example, the *light blue boxes* are provided by the magnetospheric model, which is *shaded dark blue*). The models are driven by external forcing by the Sun (i.e. solar inputs) and the lower atmosphere (i.e. tides and gravity waves)

therefore, the discrete aurora may be extremely weak. If this continues for a long time, the tail may stretch; change the characteristics of the diffuse aurora, and the ionospheric conductivity. Once a certain threshold is reached, reconnection in the tail may be allowed, and a discrete aurora may grow. This concept has been shown in simple models, but the system is even more complex than this, so it is difficult to know whether this type of feedback is of primary importance within the magnetosphere–ionosphere system. Many studies have recently been conducted in which the feedback between the high-latitude ionospheric conductivity and the magnetospheric processes have been investigated (e.g., Fedder and Lyon 1987; Ridley et al. 2004), and in the mid-latitude region, where the conductivity can strongly influence the inner magnetospheric dynamics (e.g., Ebihara et al. 2004; Liemohn et al. 2005)

The neutral wind dynamo has been known to have a strong influence on the ionospheric density structure in the equatorial and low latitude regions of the ionosphere. The neutral winds drag ions (but not electrons) across the magnetic fields, which force a closure current to form (Richmond 1995). This closure current drives electric fields (Fejer and Scherliess 1997) that can lift or push down the ionosphere, dramatically changing the vertical structure (e.g., Kelley 1989; Millward 2001; Immel et al. 2006). In the high latitudes, the same physics occurs, but the electric fields can be communicated to the entire magnetosphere. Therefore, when the high-latitude forcing is constant for many hours (ramping the neutral winds up to significant speeds), and then suddenly changes, the neutral winds may influence the magnetospheric topology through the dynamo electric fields (e.g., Deng et al. 1993; Ridley et al. 2003; Peymirat et al. 2002). This is most important for slower rotating planets, since the neutral winds are tied to a geographic coordinate system and not a sun-fixed coordinate system. On fast rotating planets, the neutrals may not have enough time to accelerate

up to appreciable speeds. On slower rotating planets (such as Earth), the neutral wind ramp-up time is approximately 3 hours (e.g., Deng and Ridley 2006), which is small enough that it allows the neutrals to stay in a region in which the acceleration is roughly constant for the full ramp-up time period. On faster rotating planets, the neutral winds may not have a constant acceleration for long enough to reach speeds in which they would strongly influence the magnetospheric convection. On the other hand, because the neutrals and ions would have very different velocities in the high latitudes on fast rotating planets, the Joule heating may be significantly larger than on Earth (e.g., Thayer and Vickrey 1992). This may energize the ions more, which may cause more ion outflow and would create more high-mass particles in the magnetospheric system.

Ion outflow at the Earth is an important source of particles in different regions of the magnetosphere. For example, the plasmaspheric density is controlled by ion outflow at Earth. Further, it has been shown that during strong activity, the plasmasheet can have a larger oxygen density, which is due to ion outflow (Young et al. 1982). At the outer planets, it is unknown what the influence of ion outflow is compared with mass loading from the moons. The direct influence of the ion outflow on the magnetospheric processes is a current subject of many studies (e.g., Winglee et al. 2005).

5.2 I-M Interaction at the Giant Planets

Generally speaking, the giant planets can interact with plasma flows from a very large region of interplanetary space, and these flows map magnetically into the ionosphere. To a first approximation, the solar wind influences plasma on magnetic field lines at the very front of the magnetosphere and on the open fieldlines in the tail and flanks. Other plasma sources and flows occur in the closed field line regions of the magnetosphere. If it is possible to study the flow of plasma in the ionosphere it is possible to derive much information about processes and mechanisms occurring in the magnetosphere itself. For Earth, such measurements can be made on a regular basis essentially *in situ*, making use of a combination of spacecraft and ground-based measurements. Spacecraft measurements of magnetospheric plasma flows are "routine" for the giant planets, but no spacecraft has so far been equipped with instruments to measure plasma flows in the ionosphere. For Jupiter, Saturn and Uranus, however, remote sensing has been developed over the past two decades making use of infrared emission from the H_3^+ molecular ion, a major constituent of giant planet ionospheres (Drossart et al. 1989; Geballe et al. 1993; Trafton et al. 1989, 1993; see reviews by Bhardwaj and Gladstone 2000; Miller et al. 2000, 2006). (So far no H_3^+ emission has not been observed from Neptune.)

Two processes modify the Dungey cycle for Jupiter and Saturn, compared with Earth. The first is the simple observation that these two planets not only have much larger magnetospheres than Earth, but that they are also spinning more than twice as fast—Jupiter rotates on its axis once every 0.41 days and Saturn every 0.44. By the time the solar wind has reached Saturn, it is traveling at ∼450 km/s. At this speed, Cowley et al. (2004) have calculated that it takes ∼70 hrs for the solar wind to traverse the Saturnian magnetosphere and return reconnected field lines from the front of the magnetosphere—where they open and connect to the IMF—back to a closed condition and returning from midnight to noon. This is approximately 6 Saturnian days as opposed the Earth's Dungey cycle which is approximately $1/8$ of an Earth day.

The second effect is one that is important for both Jupiter and Saturn, known as the Vasyliunas Cycle (see Vasyliunas 1983, for published version of this process). For Jupiter and Saturn, much of the plasma is derived from sources internal to the magnetosphere—from Io's volcanos, in the case of Jupiter, and from the rings and icy moons, in the case of Saturn.

Closed field lines, rotating rapidly with the planet, are heavily mass loaded. In the dawn–noon–dusk sectors, the loaded field lines are generally sufficiently compressed to remain intact. But as they rotate into the dusk-midnight sector, they can stretch out downtail. The mass-loaded field lines then—periodically—"pinch off" in the night-time sector, releasing "plasmoids" downtail. This is an important mechanism for ensuring that the Jovian and Saturnian magnetospheres do not become overloaded with plasma. Like the Dungey cycle, the Vasyliunas cycle is also expected to create a plasma flow signature in the ionosphere.

There is a further process that creates differences between Jupiter and Earth, and between Jupiter and (probably) Saturn, too. This is the breakdown of corotation in the equatorial plasmasheet, which produces very profound effects on Jupiter, creating its main auroral oval. Hill (1979) first described corotation breakdown at the time of Voyager. He firstly explained that Jupiter's magnetic field would drag ions produced by Io's volcanos into corotation with the planet accelerating them from 4.1×10^{-5} radians/s (the angular velocity of Io) to 1.75×10^{-4} rad/s. The momentum required to do this is supplied by the rotation of Jupiter itself: field lines passing through the plasmasheet were kept in corotation by collisions between the neutral atmosphere and ionospheric ions at the feet of the field lines. As centrifugal forces extended the plasmasheet outwards, a point is gradually reached where this mechanism is no longer able to supply sufficient momentum to maintain the magnetospheric plasma in corotation.

Two decades later came the realization that the electric fields and currents that are being generated in the middle magnetosphere, as a result of the lag to corotation in the plasmasheet, are supplying the energetic precipitating particles (mainly keV to MeV electrons, cf. Gerard et al. 1994) responsible for producing aurorae at high latitudes (Cowley and Bunce 2001; Hill 2001). The lag to corotation in the middle magnetosphere not only produces auroral emission from the upper atmosphere, but also has its own signature plasma flow. Essentially, field lines that are lagging to corotation in the middle magnetosphere drag ionospheric ions westward in the planetary frame of reference around the auroral oval. The auroral emissions are due to Lyman and Werner band transitions from molecular hydrogen with total luminosity of about 10^{13} to 10^{14} W (cf., Clarke et al. 2004).

Based on their understanding of the prevailing flows in the magnetosphere, Cowley and co-workers have produced projected ionospheric flows for both Jupiter (Cowley et al. 2003) and Saturn (Cowley et al. 2004). These show ionospheric ions corotating with the planet at lower latitudes where neutral–ion collisions are sufficient to keep closed field lines passing through the equatorial plasmasheet—and the plasmasheet itself—corotating. At larger distances out in the equatorial plane of the magnetosphere, mapping to higher latitudes, however, corotation begins to break down. Although corotation breakdown may take place over a distance of several planetary radii in the plasmasheet, the (approximately dipolar) field lines that cross this region map to high latitudes, where their footprints span a relatively narrow range. Thus, significant planetary westwards ion winds are generated in a relatively narrow (in latitude) region of the atmosphere. Note that for Saturn, Cowley et al. (2004) consider that this breakdown is not sufficient to power the main auroral oval observed on Saturn, although this is disputed (Hill 2005).

The signatures of the Dungey and Vasyliunas cycles are poleward of the region of westward winds generated by corotation breakdown. The addition of the Vasyliunas cycle in this region confines ionospheric flows due to the Dungey cycle to the dawn half of the polar cap. For Saturn, in a sector of the polar region that ranges from ~09:00 local time, through dusk, round to 03:00 local times, the Dungey and Vasyliunas flows combine to produce an anti-sunward ion drift across the whole region. As a result, the return flows are confined to a rather narrow region on the dawn flank. Ishbell et al. (1984) proposed that the polar cap

should also be subject to a lag from corotation due to the restraining influence of the solar wind on the open fieldlines that connected into it. Following Ishbell et al. (1984) and Cowley et al. (2004), in the Sun-planet reference frame the angular velocity of the polar cap region may be given by:

$$\Omega_{\text{ion}} = \Omega_{\text{planet}} \mu_0 \Sigma_P{}^* V_{SW} [1 + \mu_0 \Sigma_P{}^* V_{SW}]^{-1} \tag{9}$$

where Ω_{planet} is the angular velocity of the planet, μ_0 is the permeability of free space, Σ_P^* is the *effective*, height-integrated Pedersen conductivity of the ionosphere, and V_{SW} is the solar wind velocity. The *effective* Pedersen conductivity is given by $(1 - K)\Sigma_P$, where Σ_P is the height-integrated Pedersen conductivity of the ionosphere. K is defined (see Cowley and Bunce 2001) as $(\Omega_{\text{planet}} - \Omega_{\text{neut}})/(\Omega_{\text{planet}} - \Omega_{\text{ion}})$, with Ω_{neut} is the angular velocity of the thermospheric neutrals that coexist with the ionospheric ions; K is therefore a height-integrated parameter representing the fraction of ion angular velocity, in the frame of reference that rotates with planet, that is attained by the neutrals as a result of ion-neutral collisions. The consequences of this process for planetary energetics are discussed below.

The M-I currents associated with the Dungey cycle at Jupiter might be manifested in the auroral emissions poleward of the main oval. Sporadic, flare-like UV emissions have been observed in the polar cap (Waite et al. 2001). Auroral X-ray emission has been observed from the polar regions of Jupiter with total X-ray luminosities of $\approx 10^9$ W (cf., Gladstone et al. 2002; Elsner et al. 2005) (also see chapter 7 in this book). The most likely explanation for this polar X-ray aurora is magnetospheric ions accelerated to MeV energies (Cravens et al. 2003) and originating in the magnetopause/cusp region of Jupiter's magnetoshere (Bunce et al. 2004).

Plasma flows have been measured in the ionospheres of Jupiter (Rego et al. 1999) and Saturn (Stallard et al. 2004) from the Doppler shifting of infrared emission from the H_3^+ molecular ion. The regrettable lack of spacecraft data—no mission has or is planned to fly a spectrometer of sufficiently high spectral resolution to measure the ion Doppler shifts—can lead to some ambiguity, as it is only possible to measure velocities in the Earth-planet line of sight, and then make reasonable assumptions about the most likely flow directions. Another issue is which reference frame is the more suitable to represent measured flows: for magnetosphere–ionosphere coupling, and the tracing of magnetospheric plasma flows onto the planet itself, the inertial (Sun-planet) frame of reference is usually used; energy considerations are often better understood by making use of the frame of reference corotating with (the magnetic field of) the planet itself.

The first measurements for Jupiter (Rego et al. 1999) identified an electrojet flowing around the auroral oval, which was associated with the lag to corotation of field lines crossing the equatorial plasmasheet in the middle magnetosphere. Subsequent work by Stallard et al. (2001, 2003) identified auroral oval winds of 0.5 km/s to 1.5 km/s. Poleward of the main Jovian oval, they found near corotation in the polar region, known as the swirl region from UV measurements (Clarke et al. 2004) or Bright Polar Region from IR measurements (Stallard et al. 2001). In the region known as the Dark Polar Region from the IR measurements, a sector that was essential stagnant with respect to the magnetic pole was identified (Cowley et al. 2003; Stallard et al. 2003), which also turned out to be nearly collocated with the polar cap identified from UV measurements (Pallier and Prangé 2004).

The Saturn, measurements carried out in 2003 found a significant lag to corotation right across the auroral/polar region, such that the ion angular velocity, Ω_{ion}, was $\sim 1/3$ that of the planet, Ω_{Sat}, in the inertial reference frame (Stallard et al. 2004). On average, the value of $\Omega_{\text{ion}}/\Omega_{\text{Sat}}$ appears to be ~ 0.43 (Stallard et al. 2007a), compared with the value of 0.25, estimated theoretically by Cowley et al. (2004). From Ishbell et al. (1984), one might deduce

$V_{SW} = 600$ km/s, if the effective Pedersen conductivity is 1 mho. Later work has shown that the velocity profile may be subdivided into regions of greater or less lag to corotation, and that the polar cap itself often has a central region that (nearly) corotates with the planet. This corotating central region has been interpreted as that part of the polar cap that is connected to field lines that stretch so far down tail before reconnecting to the solar wind that they are virtually free to twist as the planet rotates (Stallard et al. 2007b). So far, it has not been possible to observe the flows that would be associated with the Dungey or Vasyliunas cycles either for Jupiter or Saturn.

As described above, current systems in the magnetosphere, generated by plasma drifts, are carried by the magnetic field lines into the upper atmosphere, where they close through the ionosphere. These ionospheric currents can heat the whole upper atmosphere via Joule heating (Waite et al. 1983). In the auroral/polar regions, where the planet's magnetic field is nearly vertical, electric fields may be estimated from the measured ion flows. For Jupiter, the magnetic field is $\sim 10^{-3}$ Tesla. Thus the measured westward (in the planetary reference frame) ion winds of between 0.5 km/s and 1.5 km/s imply an equatorward electric field given by:

$$E_{eq} = B_{aur} v_{ion} \sim 0.5\text{–}1.5 \text{ V/m}. \tag{10}$$

Joule heating is then given simply by:

$$H_J = {E_{eq}}^2 \Sigma_P \tag{11}$$

where Σ_P is the height integrated Pederson conductivity. Millward et al. (2002) have shown that the Jovian Pedersen conductivity, Σ_P, is $\sim$1–8 mho for realistic fluxes of precipitating electrons, which implies local Joule heating rates between 0.25 W/m^2 to 18 W/m^2. However, the flow of ions around the auroral oval generates a westwards neutral wind (Miller et al. 2000), which can reach velocities of between 0.5 and 0.7 of the ion velocity (Millward et al. 2005), i.e. the K parameter defined above is between 0.5 and 0.7. In this case, the effective electric field, in the frame of reference fixed to the neutral atmosphere in the auroral regions, is given by $(1 - K)E_{eq}$, where K is the parameter defined by Cowley and Bunce (2001), equivalent to v_{neut}/v_{ion} in the planetary reference frame. Thus the net Joule heating becomes:

$$H_J = [(1 - K)E_{eq}]^2 \Sigma_P. \tag{12}$$

This reduction in Joule heating, as a result of steady ion-neutral coupling, has also been noted for Earth (Thayer 1998). However, the ion drag generated by the flow of neutrals in the auroral oval against the rest of the neutral atmosphere also contributes to heating, given by (Smith et al. 2005):

$$H_D = K(1 - K){E_{eq}}^2 \Sigma_P. \tag{13}$$

Thus the total heating generated by the ions drifts and magnetospherically generated electric field is:

$$H_{Elec} = (1 - K){E_{eq}}^2 \Sigma_P. \tag{14}$$

Integrated across Jupiter's auroral/polar regions, this gives rise to heating of several times 10^{14} W, at least an order of magnitude greater than the heating due to particle precipitation, which is—in turn—an order of magnitude greater than the total solar EUV radiation absorbed planetwide. For Saturn, the total energy generated is less—by several TW—but this is still greater than heating due to particle precipitation or solar EUV.

More than two decades ago, Waite et al. (1983) questioned whether Joule (and ion drag) heating from the auroral/polar regions of the giant planets could be transferred equatorward, helping to explain the high exospheric temperatures (see Strobel and Smith 1973; Yelle and Miller 2004). Modeling carried out for Jupiter (Bougher et al. 2005) suggests that this may be possible. However, a recent study by Smith et al. (2007) for Saturn indicates that the Coriolis forces generated by the westward flowing neutral atmosphere in the auroral/polar regions turn the heated upper atmosphere poleward, rather than equatorward, and that the heat generated by Joule heating and ion drag is then mainly deposited in the lower atmosphere, rather than further heating the upper atmosphere as a whole.

6 Summary

Understanding the processes involved in the interaction of solar system bodies (planets or satellites) with plasma flows (solar wind/magnetospheric plasma flow) is fundamental to the entire field of space physics. The interaction of solar wind/magnetospheric plasma flow with weakly magnetized or unmagnetized planet/satellite is primarily an ionospheric-atmospheric interaction. Observations as well as various kinds of models have greatly enhanced our knowledge of the properties of such plasma interaction. However, there are still significant uncertainties concerning the nature of the interaction, especially when the obstacle is weakly magnetized or unmagnetized. More detailed analysis of observational data combined with improved model calculations will help to increase our current understanding of the important, controlling interaction processes.

References

M.H. Acuna et al., Science **279**, 1676–1680 (1998). doi:10.1126/science.279.5357.1676 Medline
M.H. Acuna, J.E.P. Connerney, P. Wasilewskii et al., Science **284**, 794–798 (1999). doi:10.1126/science.284.5415.794 Medline
K. Altwegg, H. Balsiger, J. Geiss, Space Sci. Rev. **90**, 3 (1999). doi:10.1023/A:1005256607402
C.S. Arridge et al., J. Geophys. Res. **111**, A11227 (2006). doi:10.1029/2005JA011574
C.S. Arridge et al., Warping of Saturn's magnetospheric and magnetotail current sheets. J. Geophys. Res. (2008, in press)
T. Bagdonat, U. Motschmann, J. Comput. Phys. **183**, 470–485 (2002a). doi:10.1006/jcph.2002.7203
T. Bagdonat, U. Motschmann, Earth Moon Planets **90**, 305–321 (2002b). doi:10.1023/A:1021578232282
H. Backes et al., Science **308**, 992 (2005). doi:10.1126/science.1109763 Medline
S. Barabash et al., Nature **450**, 650–653 (2007a). doi:10.1038/nature06434
S. Barabash et al., Planet. Space Sci. **55**, 1772–1792 (2007b). doi:10.1016/j.pss.2007.01.014
M. Benna, P. Mahaffy, Planet. Space Sci. **55**, 1031–1043 (2007). doi:10.1016/j.pss.2006.11.019
C. Bertucci et al., Geophys. Res. Lett. **30**(2), 1099 (2003). doi:10.1029/2002GL015713
C. Bertucci et al., Geophys. Res. Lett. **34**, L24S02 (2007). doi:10.1029/2007GL030865
A. Bhardwaj, G.R. Gladstone, Rev. Geophys. **38**, 295–353 (2000). doi:10.1029/1998RG000046
T. Bonev, K. Jockers, Icarus **107**(2), 335–357 (1994). doi:10.1006/icar.1994.1028
A. Bösswetter et al., Ann. Geophys. **22**, 4363–4379 (2004)
S.W. Bougher et al., J. Geophys. Res. **110**, E04008 (2005). doi:10.1029/2003JE002230
L.H. Brace et al., J. Geophys. Res. **85**, 7663–7678 (1980). doi:10.1029/JA085iA13p07663
L.H. Brace, A.J. Kliore, Space Sci. Rev. **55**, 81 (1991). doi:10.1007/BF00177136
L.H. Brace, R.E. Hartle, R.F. Theis, Adv. Space Res. **16**, 99 (1995). doi:10.1016/0273-1177(95)00255-D
J.C. Brandt, Observations and dynamics of plasma tails, in *Comets*, ed. by L.L. Wilkening (The University of Arizona Press, Tucson, 1982), pp. 519–537
J.C. Brandt et al., Icarus **137**, 69–83 (1999). doi:10.1006/icar.1998.6030
J.C. Brandt, R.D. Chapman, *Introduction to Comets*, 2nd ed. (Cambridge University Press, Cambridge, UK, 2004), Chapter 4
A. Brekke, J.R. Doupnik, P.M. Banks, J. Geophys. Res. **79**, 3773 (1974). doi:10.1029/JA079i025p03773

E.J. Bunce, S.W.H. Cowley, J.A. Wild, Ann. Geophys. **21**, 1709–1722 (2003)
E.J. Bunce, S.W.H. Cowley, T.K. Yeoman, J. Geophys. Res. **109**, A09S13 (2004). doi:10.1029/2003JA010280
R.W. Carlson, Science **283**, 820–821 (1999). doi:10.1126/science.283.5403.820 Medline
J.Y. Chaufray et al., J. Geophys. Res. **112**, E09009 (2007). doi:10.1029/2007JE002915
A.F. Cheng, J.H. Waite, J. Geophys. Res. **93**, 4107–4109 (1988). doi:10.1029/JA093iA05p04107
J.T. Clarke et al., Jupiter's aurora, in *Jupiter: The Planet, Satellites and Magnetosphere*, ed. by F. Bagenal, T. Dowling, W. McKinnon (Cambridge University Press, Cambridge, 2004), pp. 639–670
P.A. Cloutier et al., in *Venus*, ed. by D.M. Hunten, L. Colin, T.M. Donahue, V.I. Moroz (University of Arizona Press, Tuscon, 1983), p. 941
A.J. Coates et al., J. Geophys. Res. **98**, 20,985–20,994 (1993). doi:10.1029/93JA02535
A.J. Coates et al., Geophys. Res. Lett. **34**, L24S05 (2007). doi:10.1029/2007GL030919
J. Connerney et al., Science **284**, 794–798 (1999). doi:10.1126/science.284.5415.794 Medline
S.W.H. Cowley, E.J. Bunce, Planet. Space Sci. **49**, 1067–1088 (2001). doi:10.1016/S0032-0633(00)00167-7
S.W.H. Cowley et al., Geophys. Res. Lett. **30**, L1220 (2003). doi:10.1029/2002GL016030
S.W.H. Cowley, E.J. Bunce, R. Prangé, Ann. Geophys. **22**, 1379–1394 (2004)
T.E. Cravens, The physics of the cometary contact surface, in Proc. of the 20th ESLAB Symposium on the Exploration of Halley's Comet, eds. B. Battrick, E.J. Rolfe, R. Reinhard. ESA SP-250, **1**, 241 (1986)
T.E. Cravens, A magnetohydrodynamical model of the inner coma of comet Halley. J. Geophys. Res. **94**, 15025 (1989). doi:10.1029/JA094iA11p15025
T.E. Cravens, Plasma processes in the inner coma, in *Comets in the Post-Halley Era*, ed. by R.L. Newburn Jr., M. Neugebauer, J. Rahe (Kluwer, Dordrecht, 1991a), pp. 1211–1258
T.E. Cravens, Collisional processes in cometary plasmas, in *Cometary Plasma Processes*. American Geophysical Union Monograph, vol. 61 (AGU, Washington, 1991b), p. 27
T.E. Cravens, *Physics of Solar System Plasmas* (Cambridge University Press, Cambridge, 1997a)
T.E. Cravens, Geophys. Res. Lett. **24**, 105 (1997b). doi:10.1029/96GL03780
T.E. Cravens et al., J. Geophys. Res. **108**(A12), 1465 (2003). doi:10.1029/2003JA010050
T.E. Cravens et al., Composition of Titan's ionosphere. Geophys. Res. Lett. **33**, L07105 (2006). doi:10.1029/2005GL025575
T.E. Cravens et al., Geophys. Res. Lett. **35**, L03103 (2008). doi:10.1029/2007GL032451
G.K. Crawford et al., VLF imaging of the Venus foreshock. Geophys. Res. Lett. **20**, 2801–2804 (1993). doi:10.1029/93GL01258
D.H. Crider et al., Geophys. Res. Lett. **27**(1), 45 (2000). doi:10.1029/1999GL003625
D.H. Crider et al., J. Geophys. Res. **108**(A12), 1461 (2003). doi:10.1029/2003JA009875
W. Deng et al., J. Geophys. Res. **98**(A5), 7775–7790 (1993). doi:10.1029/92JA02268
Y. Deng, A.J. Ridley, J. Geophys. Res. **111**, A09306 (2006). doi:10.1029/2005JA011368
A.J. Dessler, *Physics of the Jovian Magnetosphere* (Cambridge University Press, Cambridge, 1983)
S.S. Dolginov, V.N. Zhuzgov, Planet. Space Sci. **39**, 1493–1510 (1991). doi:10.1016/0032-0633(91)90077-N
S.S. Dolginov, V.N. Zhuzgov, V.A. Sharova, V.B. Buzin, Kosm. Issled. **16**, 827–863 (1978)
P. Drossart et al., Nature **340**, 539–541 (1989). doi:10.1038/340539a0
J.W. Dungey, Phys. Rev. Lett. **6**, 47 (1961). doi:10.1103/PhysRevLett.6.47
Edberg et al., J. Geophys. Res. (2008, in press). doi:10.1029/2008JA013096
Y. Ebihara et al., J. Geophys. Res. **109**, A08205 (2004). doi:10.1029/2003JA010351
R.C. Elphic et al., J. Geophys. Res. **86**, 11430 (1981). doi:10.1029/JA086iA13p11430
R.F. Elsner et al., J. Geophys. Res. **110**, A01207 (2005). doi:10.1029/2004JA010717
A. Eviatar et al., J. Geophys. Res. **87**, 8091 (1982). doi:10.1029/JA087iA10p08091
A. Eviatar, J.D. Richardson, J. Geophys. Res. **91**, 3299–3303 (1986). doi:10.1029/JA091iA03p03299
A. Eviatar et al., Astrophys. J. **555**, 1013–1019 (2001). doi:10.1086/321510
J.A. Fedder, J.G. Lyon, Geophys. Res. Lett. **14**, 880 (1987). doi:10.1029/GL014i008p00880
B.G. Fejer, L. Scherliess, J. Geophys. Res. **102**(A11), 24,047–24,056 (1997). doi:10.1029/97JA02164
J.L. Fox et al., Space Sci. Rev. (2008, this issue)
A.A. Galeev et al., Quasi linear theory of the ion cyclotron instability and its application to the cometary plasma, in *Cometary Plasma Processes*, 2nd edn., ed. by A.D. Johnstone. Geophys. Monogr. Ser., vol. 61 (AGU, Washington, 1991), pp. 223–240
T.R. Geballe, M.-F. Jagod, T. Oka, Astrophys. J. **408**, L109–L112 (1993). doi:10.1086/186843
J.C. Gerard et al., Science **266**(5191), 1675–1678 (1994). doi:10.1126/science.266.5191.1675 Medline
G.R. Gladstone et al., A pulsating auroral X-ray hot spot on Jupiter. Nature **415**, 1000 (2002). doi:10.1038/4151000a Medline
T.I. Gombosi et al., J. Geophys. Res. **101**, 15233–15252 (1996). doi:10.1029/96JA01075
T.I. Gombosi et al., MHD simulation of comets: The plasma environment of comet Hale-Bopp. Earth Moon Planets **79**, 179 (1997). doi:10.1023/A:1006289418660

G. Gloeckler et al., Nature **404**, 576–578 (2000). doi:10.1038/35007015 Medline
Grebowsky et al., Geophys. Res. Lett. **20**, 2735–2738 (1993). doi:10.1029/93GL02239
R.M. Häberli et al., Icarus **130**(2), 373–386 (1997). doi:10.1006/icar.1997.5835
K.C. Hansen et al., Space Sci. Rev. **128**, 133–166 (2007). doi:10.1007/s11214-006-9142-6
E.M. Harnett, R.M. Winglee, Three-dimensional multifluid simulations of ionospheric loss at Mars from nominal solar wind conditions to magnetic cloud events. J. Geophys. Res. **111**, A09213 (2006). doi:10.1029/2006JA011724
R.E. Hartle et al., J. Geophys. Res. **87**, 1383 (1982). doi:10.1029/JA087iA03p01383
R.E. Hartle et al., Geophys. Res. Lett. **33**, L08201 (2006a). doi:10.1029/2005GL024817
R.E. Hartle et al., Planet. Space Sci. **54**, 1211 (2006b). doi:10.1016/j.pss.2006.05.029
T.W. Hill, J. Geophys. Res. **84**, 6554–6558 (1979). doi:10.1029/JA084iA11p06554
T.W. Hill, J. Geophys. Res. **106**, 8101–8108 (2001). doi:10.1029/2000JA000302
T.W. Hill, Rotationally driven dynamics in the magnetospheres of Jupiter and Saturn, in *Magnetospheres of the Outer Planets*, Leicester, 12 August, 2005
D.P. Hinson et al., J. Geophys. Res. **103**, 29,343–29,357 (1998). doi:10.1029/98JA02659
R.R. Hodges, J. Geophys. Res. **105**, 6971–6981 (2000). doi:10.1029/1999JE001138
R.R. Hodges, Geophys. Res. Lett. **29**(3), 1038 (2002). doi:10.1029/2001GL013853
D.E. Huddleston et al., Mass loading and velocity diffusion models for heavy pickup ions at comet Grigg-Skjellerup. J. Geophys. Res. **98**(A12), 20,995–21,002 (1993). doi:10.1029/93JA02531
W.F. Huebner et al., in *Comets in the Post-Halley Era*, ed. by R.L. Newburn Jr., M. Neugebauer, J. Rahe (Kluwer, Dordrecht, 1991), pp. 907–936
T.J. Immel et al., Geophys. Res. Lett. **33**, L15108 (2006). doi:10.1029/2006GL026161
W.-H. Ip, W.I. Axford, Nature **325**, 418 (1987). doi:10.1038/325418a0
W.-H. Ip, in *Comets II*, ed. by M.C. Festou, H.U. Keller, H.A. Weaver (Univ. of Arizona Press, Tucson, 2004), pp. 605–629
J. Ishbell, A.J. Dessler, J.H. Waite Jr., J. Geophys. Res. **89**, 10716 (1984). doi:10.1029/JA089iA12p10716
Y.-D. Jia et al., J. Geophys. Res. **112**, A05223 (2007). doi:10.1029/2006JA012175
R.E. Johnson, Energetic Charged-Particle Interactions with Atmospheres and Surfaces, 1990
R.E. Johnson et al., Space Sci. Rev. (2008, this issue)
G.H. Jones, A. Balogh, T.S. Horbury, Nature **404**, 574 (2000). doi:10.1038/35007011 Medline
E. Kallio, P. Janhunen, J. Geophys. Res. **107**(A3) (2002). doi:10.1029/2001JA000090
E.I. Kallio et al., Geophys. Res. Lett. **34**, L24S09 (2007). doi:10.1029/2007GL030827
W.T. Kasprzak, H.B. Niemann, Planet. Space Sci. **30**, 1107 (1982). doi:10.1016/0032-0633(82)90121-0
W.T. Kasprzak et al., J. Geophys. Res. **96**, 11,175 (1991). doi:10.1029/91JA00677
M.C. Kelley, *The Earth's Ionosphere: Plasma Physics and Electrodynamic* (Academic Press, San Diego, 1989)
K.K. Khurana, The configuration of Jupiter's magnetosphere, in *Jupiter*, ed. by F. Bagenal, T. Dowling, W. Mckinnon (Cambridge University Press, Cambridge, 2004)
J. Kim et al., J. Geophys. Res. **103**, 29339–29342 (1998). doi:10.1029/98JA02727
A.J. Kliore, Radio occultation observations of the ionospheres of Mars and Venus, in *Venus and Mars: Atmospheres, Ionospheres and Solar Wind Interactions*. Geophys. Monograph, vol. 66 (American Geophysical Union, Washington, 1992), p. 265
A.J. Kliore et al., Science **277**, 355 (1997). doi:10.1126/science.277.5324.355 Medline
A.J. Kliore et al., J. Geophys. Res. **107**, pp. SIA 19–1 (2002)
A.J. Kliore et al., American Geophysical Union, Fall Meeting 2007, abstract #P51D-04 (2007)
W.C. Knudsen et al., J. Geophys. Res. **85**, 7803–7810 (1980). doi:10.1029/JA085iA13p07803
C. Konz, G.T. Birk, H. Lesch, Astron. Astrophys. **415**, 791–802 (2004). doi:10.1051/0004-6361:20031695
S.A. Ledvina et al., Adv. Space Res. **26**, 1691 (2000). doi:10.1016/S0273-1177(00)00075-2
S.A. Ledvina et al., J. Geophys. Res. **110**, A06211 (2005). doi:10.1029/2004JA010771
S.A. Ledvina et al., Space Sci. Rev. (2008, this issue)
M.W. Liemohn et al., J. Geophys. Res. **110**, A12S22 (2005). doi:10.1029/2005JA011109
C.J. Lindgren Jr., T.E. Cravens, S.A. Ledvina, J. Geophys. Res. **102**, 17395 (1997). doi:10.1029/97JA01117
A.S. Lipatov, K. Sauer, K. Baumgärtel, Adv. Space Res. **20**, 279–282 (1997). doi:10.1016/S0273-1177(97)00547-4
A.S. Lipatov, U. Motschmann, T. Bagdonat, Planet. Space Sci. **50**, 403–411 (2002). doi:10.1016/S0032-0633(02)00004-1
C.M. Lisse et al., Science **274**, 205–209 (1996). doi:10.1126/science.274.5285.205
A.J. Lovell et al., Earth Moon Planets **77**, 253–258 (1999). doi:10.1023/A:1006285703521
J.G. Luhmann et al., Geophys. Res. Lett. **10**, 655 (1983). doi:10.1029/GL010i008p00655
J.G. Luhmann, Space Sci. Rev. **44**, 241 (1986). doi:10.1007/BF00200818
J.G. Luhmann, T.E. Cravens, Space Sci. Rev. **55**, 201–274 (1991). doi:10.1007/BF00177138

J.G. Luhmann, J.U. Kozyra, Dayside pickup oxygen ion precipitation at Venus and Mars: Spatial distributions, energy deposition and consequences. J. Geophys. Res. **96**(A4), 5457–5467 (1991). doi:10.1029/90JA01753
J.G. Luhmann, S.A. Ledvina, C.T. Russell, Induced magnetospheres. Adv. Space Res. **33**(11), 1905–1912 (2004). doi:10.1016/j.asr.2003.03.031
J.G. Luhmann, W.T. Kasprzak, C.T. Russell, J. Geophys. Res. **112**(E04S10) (2007). doi:10.1029/2006JE002820
E.T. Lundberg, AGU, Fall Meeting, abstract #P43A-0957 (2005)
R. Lundin et al., Nature **341**, 609–612 (1989). doi:10.1038/341609a0
R. Lundin et al., Geophys. Res. Lett. **17**, 873 (1990). doi:10.1029/GL017i006p00873
Y. Ma et al., J. Geophys. Res. **107**(A10), 1282 (2002). doi:10.1029/2002JA009293
Y. Ma et al., J. Geophys. Res. **109**, A07211 (2004). doi:10.1029/2003JA010367
Y. Ma et al., J. Geophys. Res. **111**, A05207 (2006). doi:10.1029/2005JA011481
Y.J. Ma, A.F. Nagy, Geophys. Res. Lett. **34**, L08201 (2007). doi:10.1029/2006GL029208
Y.J. Ma et al., Geophys. Res. Lett. **34** (2007a). doi:10.1029/2007GL031627
Y. Ma et al., AGU Fall Meeting, abstract #P51D-03 (2007b)
D.J. McComas et al., J. Geophys. Res. **91**, 7939 (1986). doi:10.1029/JA091iA07p07939
M.A. McGrath et al., in *Satellite Atmospheres in Jupiter: The Planet, Satellites, and Magnetosphere*, ed. by F. Bagenal, T. Dowling, W. McKinnon (Cambridge University Press, Cambridge, 2004), pp. 457–483
M. Michael, R.E. Johnson, Planet. Space Sci. **53**, 1510–1514 (2005). doi:10.1016/j.pss.2005.08.001
S. Miller et al., Philos. Trans. R. Soc. **358**, 2485–2502 (2000). doi:10.1098/rsta.2000.0662
S. Miller et al., Philos. Trans. R. Soc. **364**, 3121–3137 (2006). doi:10.1098/rsta.2006.1877
G.H. Millward, J. Geophys. Res. **106**(A11), 24,733–24,744 (2001). doi:10.1029/2000JA000342
G.H. Millward et al., Icarus **160**, 75–107 (2002). doi:10.1006/icar.2002.6951
G.H. Millward et al., Icarus **173**, 200–211 (2005). doi:10.1016/j.icarus.2004.07.027
D.L. Mitchell et al., Geophys. Res. Lett. **27**, 1871 (2000). doi:10.1029/1999GL010754
D.L. Mitchell et al., J. Geophys. Res. **106**, 23419–23427 (2001). doi:10.1029/2000JE001435
R. Modolo, G.M. Chanteur, E. Dubinin, A.P. Matthews, Ann. Geophys. **23**, 433 (2005)
R. Modolo et al., Geophys. Res. Lett. **34**, L24S07 (2007a). doi:10.1029/2007GL030489
R. Modolo et al., Geophys. Res. Lett. **34**, L24S04 (2007b). doi:10.1029/2007GL030482
U. Motschmann, K. Glassmeier, J. Geophys. Res. **98**, 20,977–20,983 (1993). doi:10.1029/93JA02533
I. Müller-Wordarg et al., Space Sci. Rev. (2008, this issue)
A.F. Nagy et al., Space Sci. Rev. **111**(1–2), 33–114 (2004). doi:10.1023/B:SPAC.0000032718.47512.92
A.F. Nagy, T.E. Cravens, Planet. Space Sci. **46**(9–10), 1149 (1998). doi:10.1016/S0032-0633(98)00049-X
N.F. Ness et al., J. Geophys. Res. **87**, 1369 (1982). doi:10.1029/JA087iA03p01369
N.F. Ness et al., Adv. Space Res. **23**(11), 1879–1886 (1999). doi:10.1016/S0273-1177(99)00271-9
F.M. Neubauer, D.A. Gurnett, J.D. Scudder, R.E. Hartle, Titan's magnetospheric interaction, in *Saturn*, ed. by T. Gehrels, M.S. Matthews (Univ. Arizona Press, Tucson, 1984), pp. 760–787
F.M. Neubauer, Astron. Astrophys. **187**, 73 (1987)
F.M. Neubauer et al., J. Geophys. Res. **111**, A10220 (2006). doi:10.1029/2006JA011676
M. Neugebauer et al., Astrophys. J. **372**, 291–300 (1991). doi:10.1086/169975
M. Neugebauer et al., Astrophys. J. **673**, 629–636 (2007)
M.B. Niedner Jr., J.C. Brandt, Astrophys. J. **223**, 655–670 (1978). doi:10.1086/156299
M. Ong et al., Geophys. Res. **96**, 11,133 (1991). doi:10.1029/91JA01100
L. Pallier, R. Prangé, Geophys. Res. Lett. **31**, L06701 (2004). doi:10.1029/2003GL018041
C. Peymirat, A.D. Richmond, R.G. Roble, J. Geophys. Res. **107**(A1), 1006 (2002). doi:10.1029/2001JA900106
J.L. Phillips, J.G. Luhmann, C.T. Rusell, J. Geophys. Res. **89**, 10676 (1984). doi:10.1029/JA089iA12p10676
J.L. Phillips et al., J. Geophys. Res. **93**, 3927–3941 (1988). doi:10.1029/JA093iA05p03927
J.L. Phillips, D.J. McComas, Space Sci. Rev. **55**, 1–80 (1991). doi:10.1007/BF00177135
P. Puhl-Quinn, T.E. Cravens, J. Geophys. Res. **100**, 21631 (1995). doi:10.1029/95JA01820
D. Rego et al., Nature **399**, 121–124 (1999). doi:10.1038/20121
A.D. Richmond, J. Geomag. Geoelectr. **47**, 191 (1995)
W.D. Riedler et al., Nature **341**, 604 (1989). doi:10.1038/341604a0
A.J. Ridley et al., J. Geophys. Res. **108**(A8), 1328 (2003). doi:10.1029/2002JA009464
A.J. Ridley, T.I. Gombosi, D.L. De Zeeuw, Ann. Geophys. **22**(2), 567–584 (2004)
S.D. Rodgers et al., Physical processes and chemical reactions in cometary comae, in *Comets II*, ed. by M.C. Festou, H.U. Keller, H.A. Weaver (University of Arizona Press, Tucson, 2004), pp. 505–522
H. Rosenbauer et al., Nature **341**, 612–614 (1989). doi:10.1038/341612a0
C.T. Russell, Geophys. Res. Lett. **4**, 387–390 (1977). doi:10.1029/GL004i010p00387
C.T. Russell et al., IEEEE Trans. Geophys. Sens. **GE-18**, 32 (1980)

C.T. Russell et al., J. Geophys. Res. **93**, 5461–5469 (1988). doi:10.1029/JA093iA06p05461
C.T. Russell, Planetary magnetospheres. Sci. Prog. **75**, 93 (1991)
C.T. Russell, J.G. Luhmann, R.J. Strangeway, Planet. Space Sci. **54**, 1482–1495 (2006). doi:10.1016/j.pss.2006.04.025
C.T. Russell et al., Venus upper atmosphere and plasma environment: Critical issues for future exploration, in *Exploring Venus as a Terrestrial Planet*. Geophys. Monograph Series, vol. 175 (AGU, Washington, 2007), pp. 139–156. doi:10.1029/176GM09
J. Saur et al., J. Geophys. Res. **104**, 25,105–25,126 (1999). doi:10.1029/1999JA900304
J. Saur et al., Geophys. Res. Lett. **27**, 2893–2896 (2000). doi:10.1029/2000GL003824
M. Schmidt-Voigt, Astron. Astrophys. **210**, 433–454 (1989)
R.W. Schunk, A.F. Nagy, *Ionospheres*, 2nd edn. (Cambridge University Press, Cambridge, 2009)
H. Shinagawa, T.E. Cravens, J. Geophys. Res. **93**, 11263 (1988). doi:10.1029/JA093iA10p11263
I. Sillanpää et al., Adv. Space Res. **38**, 799–805 (2006). doi:10.1016/j.asr.2006.01.005
I. Sillanpää et al., J. Geophys. Res. **112**, A12205 (2007). doi:10.1029/2007JA012348
S. Simon et al., Geophys. Res. Lett. **34**, L24S08 (2007). doi:10.1029/2007GL029967
J.A. Slavin et al., J. Geophys. Res. **85**, 7625–7641 (1980). doi:10.1029/JA085iA13p07625
J.A. Slavin et al., J. Geophys. Res. **96**, 11,235–11,241 (1991). doi:10.1029/91JA00439
C.G.A. Smith, S. Miller, A.D. Aylward, Ann. Geophys. **23**, 1943–1947 (2005)
C.G.A. Smith et al., Nature **445**, 399–401 (2007). doi:10.1038/nature05518 Medline
W.H. Smyth, M.L. Marconi, Icarus **181**, 510–526 (2006). doi:10.1016/j.icarus.2005.10.019
T. Stallard et al., Icarus **154**, 475–491 (2001). doi:10.1006/icar.2001.6681
T.S. Stallard et al., Geophys. Res. Lett. **30**, L1221 (2003). doi:10.1029/2002GL016031
T.S. Stallard et al., Icarus **167**, 204–211 (2004). doi:10.1016/j.icarus.2003.09.006
T. Stallard et al., Icarus **189**, 1–13 (2007a). doi:10.1016/j.icarus.2006.12.027
T. Stallard et al., Icarus **191**, 678–680 (2007b). doi:10.1016/j.icarus.2007.05.016
D.F. Strobel, G.R. Smith, J. Atmos. Sci. **30**, 718–725 (1973). doi:10.1175/1520-0469(1973)030<0718:OTTOTJ>2.0.CO;2
D.F. Strobel, *Comparative Planetary Atmospheres of the Galilean Satellites, Highlights of Astronomy*, vol. 13, ed. by O. Engvold. San Francisco, CA (Astronomical Society of the Pacific, 2005) ISBN 1-58381-189-3. XXIX, p. 894
K. Szego et al., Geophys. Res. Lett. **32**, L20S05 (2005). doi:10.1029/2005GL022646
K. Szego et al., Geophys. Res. Lett. **34**, L24S03 (2007). doi:10.1029/2007GL030677
N. Terada, S. Machida, H. Shinagawa, J. Geophys. Res. **107**(A12), 1471 (2002). doi:10.1029/2001JA009224
J.P. Thayer, J. Geophys. Res. **103**, 471–487 (1998). doi:10.1029/97JA02536
J.P. Thayer, J.F. Vickrey, Geophys. Res. Lett. **19**, 265–268 (1992). doi:10.1029/91GL02868
D.V. Titov et al., Planet. Space Sci. **54**, 1336–1343 (2006). doi:10.1016/j.pss.2006.04.017
L.M. Trafton, D.F. Lester, K.L. Thompson, Astrophys. J. **343**, L73–L76 (1989). doi:10.1086/185514
L.M. Trafton et al., Astrophys. J. **405**, 761–766 (1993). doi:10.1086/172404
J.G. Trotignon et al., J. Geophys. Res. **101**(A11), 24,965–24,977 (1996). doi:10.1029/96JA01898
J.G. Trotignon et al., Planet. Space Sci. **54**, 357 (2006). doi:10.1016/j.pss.2006.01.003
W.-L. Tseng, W.-H. Ip, A. Kopp, Adv. Space Res. **42**(1), 54–60 (2008). doi:10.1016/j.asr.2008.03.009
V.M. Vasyliunas, Plasma distribution and flow, in *Physics of the Jovian magnetosphere*, ed. by A.J. Dessler (Cambridge University Press, Cambridge, 1983), pp. 395–453
D. Vignes et al., Geophys. Res. Lett. **27**, 49–52 (2000). doi:10.1029/1999GL010703
D. Vignes et al., Geophys. Res. Lett. **29**(9), 1328 (2002). doi:10.1029/2001GL014513
M.R. Voelzke et al., Earth Moon Planets **97**(3–4), 399–409 (2005). doi:10.1007/s11038-006-9073-y
J.-E. Wahlund et al., Science **308**, 986–989 (2005). doi:10.1126/science.1109807 Medline
H.Y. Wei et al., Geophys. Res. Lett. **34**, L24S06 (2007). doi:10.1029/2007GL030701
J.H. Waite Jr. et al., J. Geophys. Res. **88**, 6143–6163 (1983). doi:10.1029/JA088iA08p06143
J.H. Waite Jr. et al., Nature **410**, 787–789 (2001). doi:10.1038/35071018 Medline
J.H. Waite et al., Ion neutral mass spectrometer results from the first flyby of Titan. Science **308**, 982–986 (2005). doi:10.1126/science.1110652 Medline
R. Wegmann, Astron. Astrophys. **358**, 759–775 (2000)
R.M. Winglee, W. Lewis, G. Lu, J. Geophys. Res. **110**, A12S24 (2005). doi:10.1029/2004JA010909
O. Witasse et al., Space Sci. Rev. (2008, this issue)
R. Yelle, S. Miller, Jupiter's Ionosphere and Thermosphere, in *Jupiter: The Planet, Satellites, and Magnetosphere*, ed. by F. Bagenal, T. Dowling, W. McKinnon (Cambridge University Press, Cambridge, 2004), pp. 185–218
Y.G. Yeroshenko, Kosmicheskie Issledovania **1**, 92–105 (1979), in Russian
Y.G. Yeroshenko et al., Geophys. Res. Lett. **17**(6), 885–888 (1990). doi:10.1029/GL017i006p00885
Y. Yi et al., J. Geophys. Res. **101**(A12), 27585–27601 (1996). doi:10.1029/96JA02235

D.T. Young, H. Balsiger, J. Geiss, J. Geophys. Res. **87**, 9077–9096 (1982). doi:10.1029/JA087iA11p09077
T.-L. Zhang et al., Geophys. Res. Lett. **18**, 127–129 (1991a). doi:10.1029/90GL02723
T.-L. Zhang, J.G. Luhmann, C.T. Russell, J. Geophys. Res. **96**, 11145–11153 (1991b). doi:10.1029/91JA00088
T.-L. Zhang et al., Planet. Space Sci. **54**, 1279–1297 (2006). doi:10.1016/j.pss.2006.04.018
T.-L. Zhang et al., Nature **450**, 654–656 (2007). doi:10.1038/nature06026 Medline